Title

Proactive Design Approaches for Energy-Efficient Buildings

Author

Li, Shuyang

Publication Date

2020

Peer reviewed|Thesis/dissertation

Proactive Design Approaches for Energy-Efficient Buildings

by

Shuyang Li

A dissertation submitted in partial satisfaction of the

requirements for the degree of

Doctor of Philosophy

in

Engineering - Mechanical Engineering

in the

Graduate Division

of the

University of California, Berkeley

Committee in charge:

Professor Masayoshi Tomizuka, Chair
Professor Kameshwar Poolla
Associate Professor Anil Aswani

Fall 2019

Proactive Design Approaches for Energy-Efficient Buildings

Abstract

Proactive Design Approaches for Energy-Efficient Buildings

by

Shuyang Li

Doctor of Philosophy in Engineering - Mechanical Engineering

University of California, Berkeley

Professor Masayoshi Tomizuka, Chair

During the past years, studies have shown that energy-efficient buildings can provide effective means to achieve a range of global goals and bring multiple benefits to society, environment, and economy. As the most considerable energy and electricity consumption sector, the building industry has gradually fulfilled the vision of zero-energy or even net-positive-energy design and construction. Meanwhile, the large thermal mass and a significant amount of flexible load also make building the ideal target for energy storage and demand response to maintain grid stability. With the advent of smart devices and advanced technologies, more advanced design approaches have been developed to reduce the maintenance and utility costs while maintaining occupant comfort. In this dissertation, proactive approaches for the high-performance buildings are discussed in three phases, control system designing, monitoring-based commissioning, and existing building retrofits with renewables.

Modern buildings are equipped with monitoring systems to gather thousands of time series that capture and store real-time and historical information about occupancy, temperature, energy, and many other measurable operational data. Intelligent data analytics empower building management to transform into a predictive and proactive approach, which increases energy efficiency, improve occupant comfort, and predict maintenance. The powerful insights pulled from the data patterns enables the control strategy transformation from heuristic or rule-based to model-based.

Heating, ventilation, and air conditioning (HVAC) systems account for over 50% of the total energy use in buildings. They have enormous energy-saving potentials such that to be highlighted for commissioning and retrofitting. Chapter 2 and 3 present the physical model development for both energy and thermal dynamics within the

building envelop. Details on the simulation-based, as well as the data-driven based model identification methods, are provided in Chapter 3. Given the unavailability of measurement, parametric, semiparametric, and nonparametric models are adopted to predict the thermal loads those grey-box models achieve a balance between model interpretability and accuracy.

In Chapter 4, starting from the current best practice control strategy, demand-responsive rule-based control, in compliance with many building standards and codes, the proposed cost-responsive design strategy incorporates energy models, dynamically estimates the total cost among several candidate setpoints, and them iteratively moves in the direction of the least cost. The experiment results in Chapter 5 demonstrate the effectiveness of the proposed proactive control strategy and reveal significant energy cost reduction without compromising occupant comfort. This cost-effective approach is feasible to implement on a large scale with minimum interfering with the existing building management system infrastructure. Some practical challenges faced during deployment and testing are discussed and analyzed along with the possible generalization to other cases.

Chapter 6 documents issues and recommendations from a commissioning project concerning heating and ventilation issues arising from the occupant survey. In-depth statistical analyses of operational data trends over time can inform the possible fault and provide insights for future proactive maintenance. The case study demonstrates the feasibility of proactive monitoring-based commissioning. Furthermore, parametric methods of analyzing benefit and value in terms of cost, comfort, and energy are investigated on an existing office building to evaluate energy-efficient measures for retrofitting in Chapter 7. On-site renewable energy generation can be designed to achieve zero net energy.

To my family and friends

Contents

List of Figures

List of Tables

Acknowledgments

The past few years at UC Berkeley has been a truly life-changing and memorable milestone in my life. It would not have been possible to earn a Doctorate without the support and guidance from many people. Firstly, I would like to express my highest appreciation to my advisor Professor Masayoshi Tomizuka for the continuous support of my Ph.D. study and related research. He always encourages me and gives me the right suggestions when I have no clue. His patience and immense knowledge always inspire me to explore different challenging areas. Especially when I have a health problem, he shows a deep understanding and provides great support for finalizing my thesis.

I would also like to express my sincere gratitude to Professor Kameshwar Poolla and Professor Anil Aswani, who served on my dissertation committee. They provided me with constructive comments about research during the valuable discussions. Moreover, I would like to thank Professor Roberto Horowitz, Professor Francesco Borrelli, Professor Shmuel S. Oren, and Professor James Casey, who served on my qualifying committee. Their examination and approval made me confident to continue my studies and research.

I want to thank Professor Duncan Callaway, Professor Stefano Schiavon, Paul Raftery, Brendon Levitt for their tremendous help on the simulation and experimental tests. They shared their industry experience with me and gave practical suggestions to my research. I also want to thank Domenico Caramagno for his help in facilitating the experiments.

It is a great honor to have so many friends and colleagues to share life and experience. I want to thank Cheng Peng, Baihong Jin, and Ting Ming for all the valuable discussions and efforts towards projects. I would also like to thank all members of the MSC lab for being there throughout the years, encouraging when I feel overwhelmed.

Finally, my deepest love and appreciation go to my parents for their unconditioned and endless support.

Chapter 1

Introduction

1.1 Backgrounds

According to the U.S. Energy Information Administration (EIA)[1] and the Environmental Protection Agency (EPA) [2], the building sector accounted for about 40% of total U.S. primary energy consumption and 72% of total U.S. electricity consumption over their life-cycle. The energy is mostly derived from fossil sources that produce the carbon dioxide which is the main cause of global warming. The building sector was responsible for nearly 40% of U.S. greenhouse gas emissions. Necessary steps need to be taken to preserve livable conditions on earth. Architecture 2030 [3] provides the high-impact actions to transform the built environment to carbon-neutral by 2050. The green building idea raises as a solution with social, economic, and environmental benefits, which changing traditional practices towards a more sustainable future. The green building benefits are quantified by the General Services Administration (GSA) [4] as 13% lower maintenance costs, 26% less energy usage, 27% higher level of occupant satisfaction, and 33% lower CO2 emissions. The solutions comprise several parallel paths: increase the energy efficiency of the building stock, replace polluting sources with clean and renewable energy sources.

The three-tier sustainable design approach introduced in [5] states that first two tiers, basic building design, and passive systems, are the domain of architects, and proper design decisions can reduce the energy consumption of buildings as much as 80%. Tier three requires designing the mechanical and electrical systems by engineers to be as efficient as possible. Thus, only 15% as much energy is needed in a properly designed building as in a conventional building. Over the years, researchers have learned how to design, build, and operate "zero-energy buildings" (ZEB)[6, 7, 8], which uses as little energy as possible, with the small remaining load being met

mostly by on-site renewable energy such as photovoltaics on the roof.

However, there are a large number of existing buildings that do not meet the energy efficient requirement at the first two tiers due to many reasons. The most common reason is the neglect of climate characteristics. There are buildings designed with large glazed areas to improve the aesthetics in very hot or very cold climates. The engineers then have to design bulky, energy-guzzling mechanical systems to maintain thermal comfort. Heating, ventilation, and air conditioning (HVAC) account for nearly 45% of the total site energy consumption in both residential and commercial buildings [1]. Its apparent predominance reveals the significant importance of optimal design and control for both existing and future buildings.

1.2 Literature review

HVAC system consists of three parts: heating, cooling, and ventilation [5]. There are several types of heating systems, for example, electric heating, hot-water heating, hot-air heating, and heat pumps. As for air-conditioning systems, there are through-the-wall units (PTAC), packaged systems, split systems, and ductless split systems for small buildings, while all-air systems, all-water systems, and combination air-water systems for large buildings. The air distribution systems can be categorized as single-duct and double-duct systems. Therefore, there are many variations in system design to meet different purposes and requirements.

HVAC system control involves designing optimal sequence for many controllable setpoints, such as comfort temperature range, supply air temperature, ventilation flow rate, economizer position, etc [9, 10, 11, 12, 13, 14]. The standard practices are suggested and required by standards and codes [15, 16, 17, 18]. With the advent of Direct Digital Control (DDC) and advances in data storage, computing, and communication devices, more complex control strategies have been developed and implemented in testbeds to validate the efficiency and to provide guidance for future best industrial practice.

Model Predictive Control (MPC) is shown in considerable work to outperform existing production logic in terms of lower energy consumption, better transient response, robustness to disturbances, and adaptive to varying conditions [19, 20, 21, 22, 23]. The main idea of predictive control is to use a model of the plant to predict the future evolution of the system. At the current time step, an open-loop optimal control problem is solved over a time horizon. Only the first optimal command signal is applied to the system. At the next time step, a new optimal control problem based on the new state is solved over a shifted horizon.

Similar to any other model-based method, MPC has the following problem: the performance highly depends on the accuracy of the model, disturbance prediction. [24] shows a 20% cost difference between the best performing model and the worst performing model for the cases studied. The computation complexity is also another liability. It is essential to choose an appropriate prediction horizon and sampling time. Cascade MPC is designed to solve the discrepancy between slow dynamics and fast-moving disturbances. Two-mass system models consisting of fast (air temperature) and slow (wall temperature) dynamics are advocated in [25, 21]. The idea is motivated from the lagging phenomenon: in the morning, cold walls which represent the slow dynamics with high heat capacity will be warmed up using most of the solar radiation; in the afternoon, walls absorb heat at a slower rate which causes faster increasing of the air temperature in the thermal zone. The time-of-use electricity price hierarchy can then be integrated into MPC design, which enables the peak shifting by pre-heating or pre-cooling.

The area of decentralized control is created to address the challenges arising in the control of real-world systems with many interconnected subsystems. A set of partially interacting local controllers is designed to reduce computation or communication complexity. Distributed control is similar to decentralized control but with some information exchange between the local controllers. However, the previously designed Distributed Model Predictive Control (DMPC) in buildings has substantial communication overhead using Sequential Quadratic Programming (SQP) and dual decomposition [20, 26].

Compared to the traditional reactive design approach, which just reacting to current conditions, proactive design strategies with the capability of acting in advance of a future situation have many advantages: increased energy efficiency, improved occupancy comfort, increased operational efficiency, and better predictive maintenance. A proactive building intelligence solution usually involves predicting thermal loads throughout operational hours and regulating temperature levels before they spike. Studies have shown that incorporating occupancy behavior and solar energy exploitation with existing building management systems can both reduce energy consumption and improve occupant comfort compared to the baseline reactive control [27, 28, 29]. One representative proactive control product is the Comfy Insights [30], which allows building occupants to make individual heating or cooling requests based on their comfort needs and then dynamics adjust temperature set points and ranges according to occupant preference learned from historical requests with up to 25% energy savings. Studies on predictive maintenance [31] have shown 30% maintenance costs reduction, 75% of the breakdown time elimination, and about 40% downtime reduction.

1.3 Dissertation Outline

In this dissertation, the proactive design approaches for three main stages among building life-cycle to achieve energy efficiency are discussed using case studies. During the planning and design stage, optimal control strategies for the HVAC system are explored. For existing buildings, a continuous process of fault detection and diagnosis would be necessary during the maintenance and commissioning stage. Further, more cost-intensive system upgrades could be evaluated based on simulation during the renovation and retrofitting stage. The dissertation is organized as follows.

Chapter 2 presents the energy models and comfort indexes used in the control design for the typical single-duct central-cooling systems with reheat modules. Without direct measurement from the water-side (i.e., chilled water and hot water), a modified air side heat balance using available sensor data is performed to estimate the intentional cooling and reheat energy use. The energy consumption of the supply air fan, which circulates the cooled air throughout buildings, is modeled using Affinity Laws. Occupancy comfort is another optimal target besides energy. Some quantified constraints over measurable variables are imposed to provide a certain level of occupant satisfaction.

Chapter 3 presents the four types of simplified models for the thermal dynamics within the building envelope. The thermal load needs to be estimated simultaneously with system dynamics parameters identification. The simulation-based approach incorporates modeling the geometry, including the layout and construction materials. The simulation engine and software toolbox are used together to obtain the system matrices of a higher-order linear system model. Three data-driven based approaches - semiparametric, parametric, and nonsupervised regression, are studied and tested on historical data collected from an office building at UC Berkeley.

Chapter 4 outlines the control strategy design for HVAC systems. The current best practice, rule-based control, is request-responsive. The control law is piece-wise linear with respect to PID output of zone temperature and outside air temperature. To perform "better than the code", model-based control strategies are investigated. A cost-responsive control strategy is proposed to incorporate the energy model. The optimal setpoint for supply air temperature for the next time step is chosen to be the one with the lowest predicted total cost.

Chapter 5 reports the detailed case study for cost-responsive control strategy implementation on the Sutardja Dai Hall at UC Berkeley. A randomized controlled trial is conducted by switching between the proposed strategy and the current baseline strategy. Experimental results suggested that the cost-responsive strategy can reduce 17% of the total cost. Some practical issues on implementation are also discussed.

Chapter 6 presents a case study of a classroom building to demonstrate how oper-

ational data can inform the possible faults during monitoring-based commissioning. The energy audit and occupancy survey can provide some information about potential problems. More insightful facts can be revealed by analyzing data patterns. After on-site examination, malfunctioning valves and passive valves are identified. Meanwhile, the root cause for the under-ventilated room is identified as the small opening of the economizer.

Chapter 7 presents a case study of an office building to demonstrate the cost evaluation of possible energy-efficient upgrade measures for a retrofitting project. The mixed-mode ventilation analysis is conducted to access the buildings potential to take advantage of natural ventilation. The desirable natural ventilation schedule can be incorporated into the current control system in order to reduce mechanical ventilation energy use while producing the highest percentage of comfortable time during occupied hours. Rooftop solar panels with different titled angles are evaluated to provide the most renewable production.

Chapter 2

System Description and Modeling

2.1 HVAC system

In practice, Building Management System (BMS) control platforms are physically distributed throughout the building. For a most common type of HVAC system in commercial buildings, single-duct VAV with reheat[1], as shown in Figure 2.1, the central processor is located at the Air Handling Unit (AHU), while the local control units are distributed at each thermal zone. Each thermal zone, served by one VAV box, can be composed of several rooms which share the same or similar thermal condition, such as temperature and humidity. There are some practical concerns about allocating thermal zones. On the one hand, although separating every room as a thermal zone will achieve higher control accuracy, it will increase the infrastructure (ductwork, damper, filter, etc.) complexity and cost as well. Therefore, some non-critical rooms, such as storage and cleaning closets, can be assigned together as one thermal zone. On the other hand, some large spaces, such as big auditoriums and hallways running through the entire building, can be separate into different thermal zones for twofold reasons: space limitation of bulky ducts for large airflow need, plus inherent distinct thermal conditions from difference exposures. In this paper, we assume that there are n thermal zones in the building, as assigned in the BMS.

The AHU circulates air through the buildings by supply and return fan. The fresh outside air and return air are mixed with proportion controlled by economizer damper. The mixed air can be cooled using chilled water when needed. Before discharging each zone, the supply air goes through VAV box first to regulate flow and temperature using heating coil and damper. Inside each zone, diffusers or registers mix discharge air and zone air without causing drafts. And the air is assumed to be at

[1] "Reheat" is called because the air is cooled down first and then warmed up.

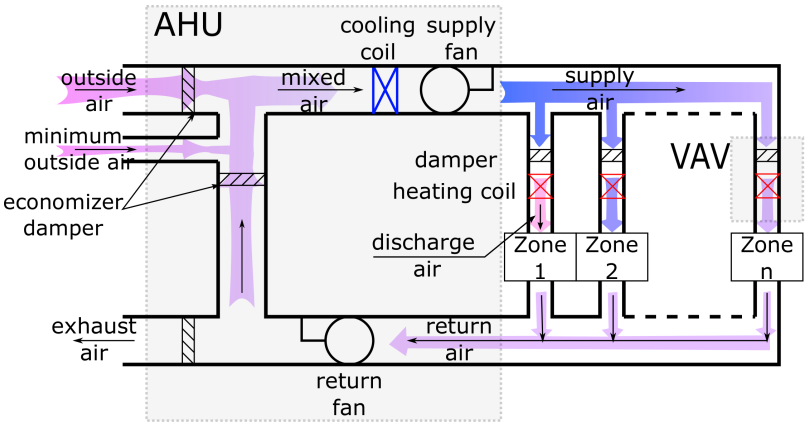

Figure 2.1: HVAC system schematic diagram

the same temperature among the space without stratification. Return air generally leaves a zone through a grille, as shown in Figure 2.2.

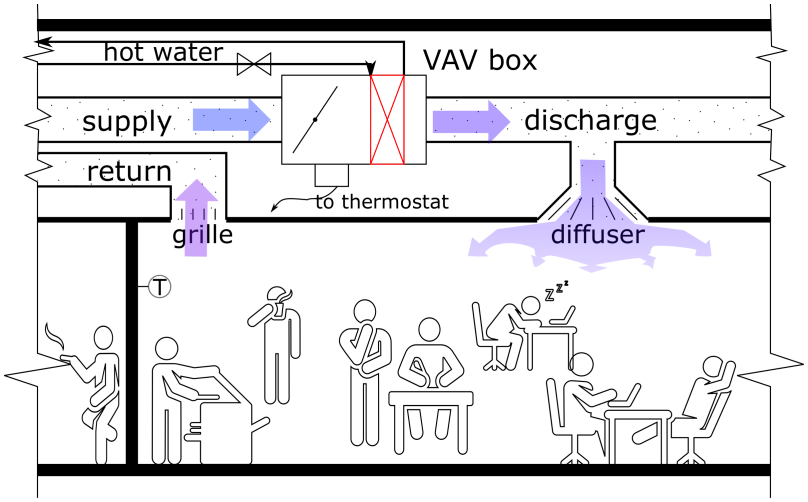

Figure 2.2: VAV system schematic diagram

In summary, the control inputs at the AHU level are: the outside airflow rate, the return airflow rate, and the cooling coil outlet temperature setpoint (i.e. supply air temperature setpoint). The control inputs at the VAV level are: the discharge airflow

rate, and the heating coil outlet temperature setpoint (i.e. discharge air temeprature setpoint).

2.2 Modeling

Assumption

The assumptions for all levels are listed below and the assumptions for specific part are detailed in each subsection.

(A1) All dynamics other than thermal dynamics of zones are neglected. That is to say, there is no measurement delay; actuators achieve their control setpoints instantaneously; air fully mixes without delay.

(A2) Humidity is not explicitly included in the model for twofold reasons: the comfort zone covers a relatively large range of relative humidity, plus it is not an issue in East Bay area.

(A3) Measurements from sensors are accurate and historical time-series data is accessible.

(A4) The air in one thermal zone is assumed to be uniform across its volume. And the thermal characteristic of the air, walls, furnishings, and other contents of zone i can be combined into a single parameter.

(A5) The air mass in the thermal zone will not change in the process, i.e. the discharge air mass flow rate equals the return air mass flow rate.

(A6) There is no air leakage in the ducts.

Measurement

There might be thousands of sensors installed in high-rise buildings: at the AHU level, supply air duct static pressure, supply/mixed/return/outside air temperature, total supply/return airflow rate, chilled water valve position, outside/return/exhaust air damper position, return air humidity (optional), etc; at the VAV level, discharge airflow rate, discharge air temperature, hot water valve position, damper position, zone temperature, zone CO_2 concentration(optional).

It is worth noting that accurate measurement of variables is critical. Take temperature sensor for example, using the same type of sensors to measure all temperatures

will help eliminate sensor calibration errors. A bulk of redundant measures may be used to improve the accuracy. Several readings may need to be taken and averaged to accurately reflect the true value. In addition, some measured variables can be also expressed using other variables, which provides a way to detect and diagnose fault when the deviation is too large.

Since the supply air mass flow rate is assumed to be equal the return air mass flow rate, the return air temperature T_r can be calculated as weighted average of zone temperature $T_{z,i}$ as

$$T_r = \sum_{i=1}^{n} \dot{m}_i T_{z,i} / \sum_{i=1}^{n} \dot{m}_i \tag{2.2.1}$$

where the total mass flow rate $\dot{m}_c$ can be denoted as the sum of discharge air mass flow rate $\dot{m}_i$

$$\dot{m}_c = \sum_{i=1}^{n} \dot{m}_i \tag{2.2.2}$$

In reality, the airflow sensors in VAV and AHU are not as accurate as temperature sensors and are subject to large variation under different inlet flow conditions. The airflow reading error could be up to 45% according to the test result in [32]. Figure 2.3 shows the difference between the total air mass flow fraction measured from AHU and VAV. Each data point is an instantaneous measurement reading from the BMS.

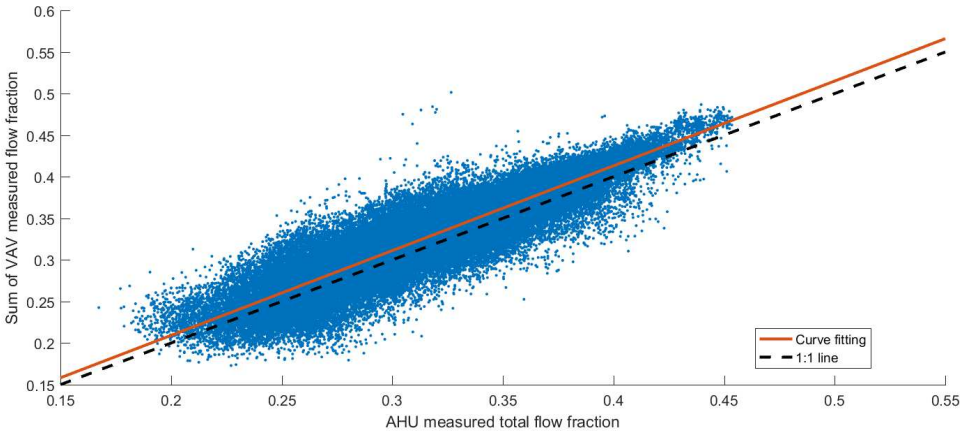

Figure 2.3: Total mass flow measurement from both AHU and VAV

Sometimes, there will be separate panel meters which measure aggregated power consumption of the same type, the same serving location, or adjacent equipments.

For instance, total power of fan system, which includes supply fan, return fan, and exhaust fan, can be recorded using substation meter.

Economizer

The economizer damper position η determines the amount proportion between the fresh outside air and the return air. Sometimes, there will be a separate minimum outside air duct which is open all the time to guarantee enough amount of fresh air during recirculation, as shown in Figure 2.1. The economizer was designed to utilize the outside air to minimize energy consumption in some situation. For example, in summer night, the outside temperature is relatively low compared to the indoor temperature. We can use 100% outside air to cool the building instead of using cooling coil, i.e. $\eta = 1$. While in winter, we want to use most warm return air to keep thermal comfort instead of using heating coil excessively, i.e. $\eta \simeq 0$ (not strictly zero because minimal outside fresh air need to be guaranteed).

Assume that perfect mixing occurs, the mixed air temperature T_m can be calculated using the outside air temperature T_o, the return air temperature T_r, as well as the proportion η

$$T_m = \eta T_o + (1 - \eta) T_r \tag{2.2.3}$$

We can also using temperature sensors to calculate η and provide feedback control. This approach works best when there are significant differences between the outdoor air temperature and the return temperature, such as in extreme hot and cold days.

Air-water heat exchanger

The heating and cooling coils are air-water heat exchangers, i.e. the chilled water (or hot water) that is acting as a heat sink (or heat source) soaks up (or gives up) heat and gets warmer (or colder) while the air gets cooler (or warmer). Taking the cooling coil for example, the supply air temperature T_s depends on the cooling valve position, the chilled water temperature, the mixed air temperature T_m, the mass flow rate of the mixed air $\dot{m}_c$, and the thermal effectiveness of the cooling coils. We assume that in the ideal case, the chilled water needs to provide cooling power P_c which equals to the power used for cooling the total supply air $\dot{m}_c$ down to a certain temperature

$$P_c = \dot{m}_c c_p (T_s - T_m) \tag{2.2.4}$$

where c_p is the specific heat capacity of air. Similarly, we assume the heating power required in the water side equals to the power needed in the air side. For each VAV

box,

$$P_{h,i} = \dot{m}_i c_p (T_{d,i} - T_s) \tag{2.2.5}$$

where $\dot{m}_i$ is the discharge air mass flow rate, and $T_{d,i}$ is the discharge air temperature.

The above coil power model makes strong assumptions: the thermal power from the water side delivers completely to the air side without any loss. In other words, we only consider the sensible heat removed by the heating and cooling coil, which is not a significant issue given the outside air dew-point.

Chiller

Chillers and cooling towers are responsible for providing chilled water by means of a vapor-compression or absorption refrigeration cycle. Usually, the chiller model and control are not taken into account since each equipment manufacturer provides unique control logic with different types of machine. As long as the chilled water temperature is set, we suppose that the chiller will provide it in real time. The water-side energy consumption can be calculated using the corresponding return and supply water temperature, as well as the chilled water flow. Alternatively, the chiller power consumption can be calculated using equation (2.2.4) in combined with the coefficient of performance (COP).

Fan

The supply and return fans are usually driven by electric motors to guarantee the required ventilation and a slightly positive pressure in the building. To reduce energy consumption and cost, variable frequency drive (VFD) is installed in most commercial buildings to allow fan controlling its motor speed with which it moves air around. The electrical input power displayed by VFD is the actual fan power consumption. Besides, according to the affinity law (also known as "fan laws"), the fan power is theoretically cubic with volumetric flow rate. A part-load factor/ratio r is first calculated as the ratio of the actual operating mass flow rate $\dot{m}_c$ to the maximum fan mass flow rate $\dot{m}_{\text{full}}$. Then a third-order polynomial model can be fitted as following using historical data.

$$P_f = a_1 r^3 + a_2 r^2 + a_3 r + a_4 \tag{2.2.6}$$

where $r = \dot{m}_c / \dot{m}_{\text{full}}$. Some reference fan curve coefficients were developed using the characteristic system curve fan model in [33]. The part load performance from curve fitting and reference is presented in Figure 2.4. Note that the y-axis is percent power which is the ratio of actual power to the maximum power. The data used for curve

fitting is collected from BMS, where the fans operate mostly in low-load situation (between 0.2 and 0.5) with static pressure reset strategy. The results show that the fitting curve coincides with the theoretical curve along the operational range as in Figure 2.3.

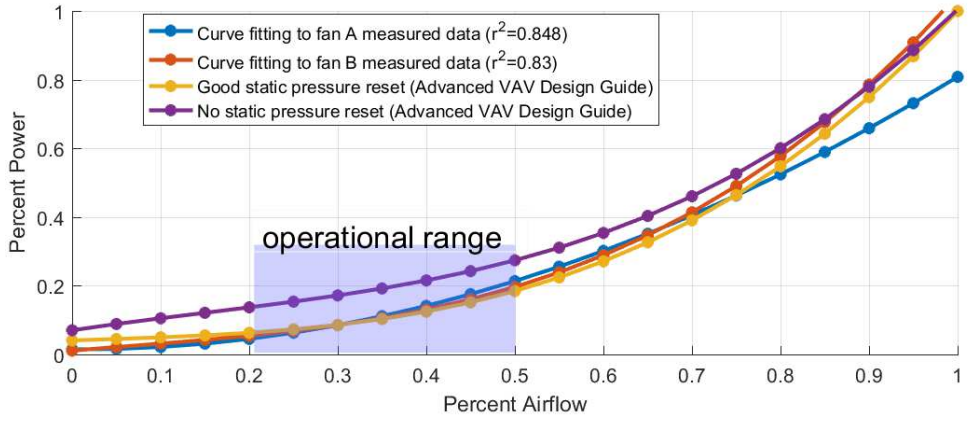

Figure 2.4: Fan part load performance

Thermal zone

The heat and mass transfer processes involved in a thermal zone include manifold forms: conduction heat transfer through the building construction elements (including walls, roof, ceiling, and floor); solar radiation transmission through windows; infiltration of outside air; heat dissipation from equipment and occupants; heating and cooling provided by the HVAC system. A valid mathematical model of thermal behavior for zones is required for all model-based optimal controls.

Traditionally, high-dimensional purely physical white-box models are developed and validated through simulation softwares, such as TRNSYS [34], EnergyPlus [35], and Modelica [36]. These complex models include all features in a building and can yield high granularity of prediction with appropriate parameter calibration. However, the large amount of tunable parameters and data make them computationally expensive and difficult to adopt in optimal control design problem.

The simplified lower-dimensional data-driven models, thus, become the focal attention of researchers. It alleviates the model and computational complexity in expense for coarse prediction within an acceptable error range. Black-box regression techniques, such as neural network [37], can lead to models that do not respect the

proper physics. Furthermore, it is not known how well the model would perform in situations that do not occur in the training data. The grey-box models that combine some physics, are favorable.

In general, the thermal dynamics of each zone are

$$\frac{dT_{z,i}(t)}{dt} = f_i(T_{z,1}(t), \cdots, T_{z,n}(t), T_{d,1}(t), \cdots, T_{d,n}(t), \dot{m}_1(t), \cdots, \dot{m}_n(t), T_o(t), T_s(t), q(t)) \tag{2.2.7}$$

where $f_i(\cdot)$ is some unknown nonlinear function, $T_{z,i}$ is the temperature in the $i-$th zone, $T_{d,i}$ is the discharge air temperature, $\dot{m}_i$ is the amount of air sent to the zone, T_o is the outdoor air temperature, T_s is the supply air temperature and q are variables related to other effects. In Chapter 3, more detailed modeling methods are introduced.

2.3 Indoor Environmental Quality (IEQ)

The ultimate goal of intelligent design and control is to better serve building occupants. Energy efficient buildings with high-quality indoor environments protect the health and comfort within the building envelop. The IEQ includes indoor air quality and thermal, visual, and acoustic comfort. However, it is challenging to quantify the comfort index as an optimization goal. Instead, some quantitative indicators are chosen to be included as optimization constraints, such as CO_2 concentration and room temperature.

In practice, occupancy survey is the most powerful method to assess the IEQ. Figure 2.5 shows the occupant survey result of three classrooms in Davis Hall. Occupant Survey Toolkit [38] developed by the Center For the Built Environment can be used to better conduct and deliver the survey result.

Thermal comfort

The thermal comfort of occupants is mainly determined by four conditions: air temperature, relative humidity (RH), air movement, and mean radiant temperature. The comfort range for most people (80%) extends from 20°C to 25°C, from 20%-80% RH in winter to 20%-60% RH in summer, from 0.1 to 0.3 m/s air motion speed [5]. The range is large because of many other variables involved, such as clothing level and metabolic rate. The comfort zone on the psychrometric chart under different conditions can be obtained using the online CBE Thermal Comfort Tool [39] as shown in Figure 2.6.

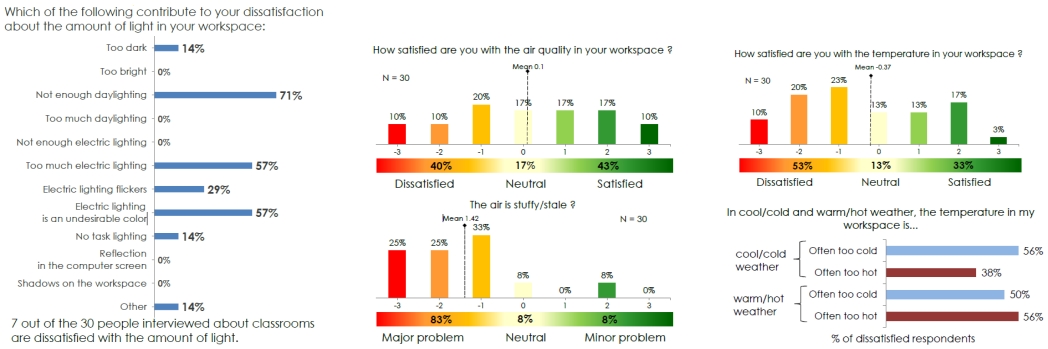

(a) Lighting (b) Air quality (c) Thermal comfort

Figure 2.5: Sample occupancy survey regarding IEQ

In most modern commercial building, only the air temperature factor is considered and controlled to infer thermal comfort. The relative humidity is sometimes controlled within a relatively wide range at central supply level, especially in humid areas. As for air speed, it would require special measurement sensors, such as omni-directional hotwire anemometers. The mean radiant temperature is also very location-dependent as the air speed. It is not practical to measure and control it for each workstation. In the following of the paper, only the air temperature is considered for the thermal comfort constraints, as shown in equation (2.3.1).

$$T_{z,i}(k) \in \mathcal{T}_i(k) = [\underline{T}_{z,i}(k), \overline{T}_{z,i}(k)] \tag{2.3.1}$$

where the default comfort range is $[21.1°\text{C}, 23.3°\text{C}]([70°\text{F}, 74°\text{F}])$. Note that the thermal comfort ranges could be different for different zones at different times with some adaptive learning programs running, such as Comfy [30]. The minimum and maximum temperatures are preset to certain values for occupied and unoccupied hours, additionally, they can be dynamically reset according to occupants' requests.

Air quality

Indoor air quality (IAQ) is often defined as the index of whether the air is fresh and pleasant. Some topics mention in [40] relative to control system are listed here: air pressure need to be 3 to 7 pascals positive with respect to outdoor air, in order to avoid unintended infiltration into the building envelope; outdoor air ventilation need to be continuous and at least the required minimum flow rates during occu-

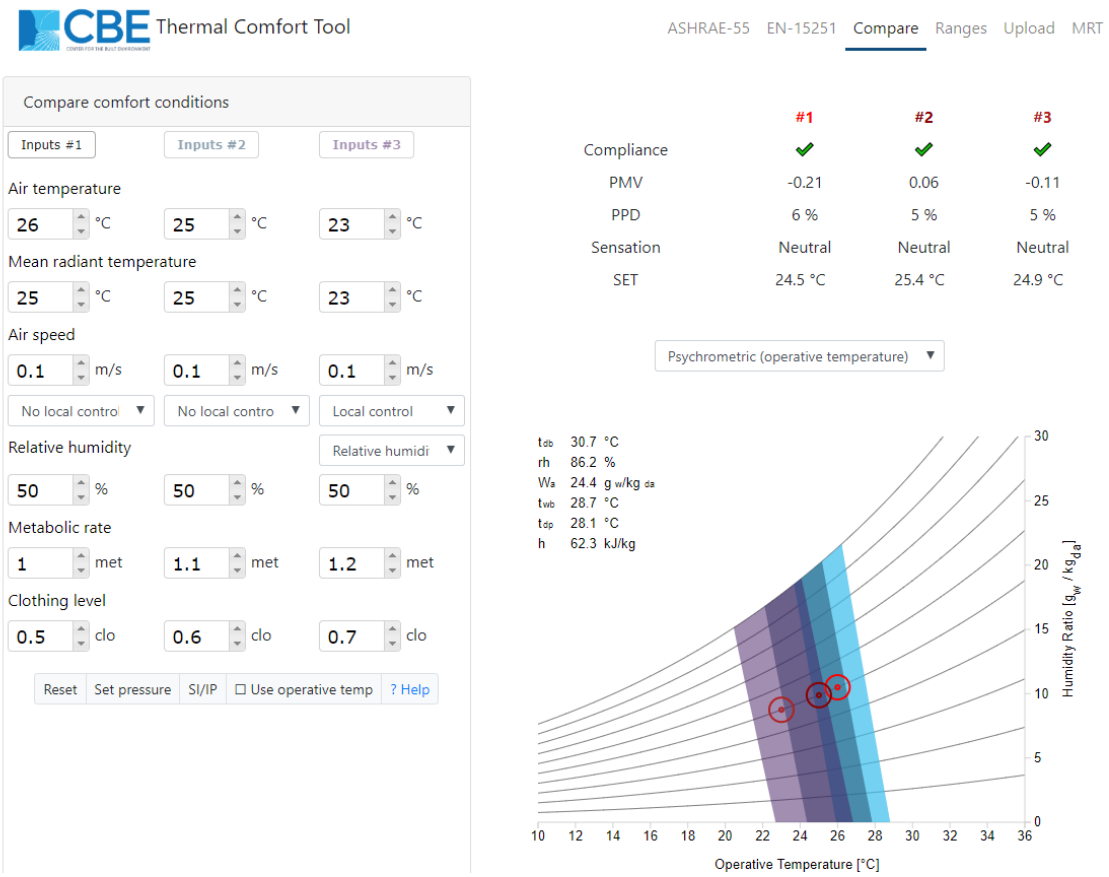

Figure 2.6: The thermal comfort range for different scenarios

pancy, in order to remove many indoor generated air contaminants from furnishings, equipment, and occupants; moisture level need to make materials dry from wet less than two days; air filtration systems need have a particle-removal efficiency at least Minimum Efficiency Reporting Value 8. In addition, CO_2 concentrations can be used as an indicator of odorous bioeffluents and occupant acceptance of these odors, with the acceptable range from 1000 to 1200 ppm. Usually, the air quality measures are not accounted for modeling.

To ensure the indoor air is healthy to breathe, there are some constraints on the control variables. The positive building pressure is not directly controlled, but is adjusted via the amount of air sucked and blown. An alert would be trigged when the building pressure drops below a certain value. Mechanical ventilation system is

required by many building codes, and the minimum outdoor air ventilation rates are also specified as in equation(2.3.2).

$$\dot{m}_i \geq \underline{\dot{m}}_i \tag{2.3.2}$$

where the minimum discharge air mass flow rate is suggested to be 15 cfm/occupant, 0.15 cfm/ft^2, or 1.0 ACH, whichever is greater [16]. Note that for unoccupied hours, there is no strict requirement on the ventilation. However, most buildings would keep the minimum flow rate to ensure the positive building pressure and better air quality at next morning.

2.4 Physical and Practical Consideration

There are many physical and practical limitations for the actuators and equipments installed in the building.

- Dampers

  The stability and accuracy of a VAV box depends on two main components: the flow probe provided by the box manufacturer, and the controller typically provided by a separate control manufacturer. It is important to make sure that the VAV boxes can achieve a given flow setpoint while the inlet pressure is fluctuating. The controllers could have some issues, such as under-estimating actual flow at minimum flow, and zero-drift which requires re-zero at certain period. Therefore, the damper command in each VAV box which controls the desired discharge airflow rate is better above 10%-20% open. It is not included in the model constraints since the damper position is the intermediate control variable.

  System engineers and air balance technician would design the minimum and maximum airflow rate for each thermal zone, and then size the proper duct and diffuser window. The minimum airflows are determined by the ventilation and controllability issues, while the maximum airflows are determined from the total pressure drop and sound power levels. Here, it is assumed that all these values are given, as expressed in equation (2.4.1).

$$\underline{\dot{m}}_i \leq \dot{m}_i \leq \overline{\dot{m}}_i \tag{2.4.1}$$

- Temperatures

The supply air temperature cannot be greater than the outdoor air temperature since there is no heating component at AHU. However, it might exceed a few degrees due to duct heating.

$$T_s^{sp} \leq T_o \tag{2.4.2}$$

The discharge air temperature cannot be lower than the supply air temperature since there is no cooling component at VAV.

$$T_d^{sp} \geq T_s \tag{2.4.3}$$

2.5 Summary

In this chapter, the building HVAC systems are presented and modeled for optimization purpose. Some quantitative indoor environmental quality are discussed to serve as optimization constraints. The thermal dynamic model for each zone will be presented in more detail in next chapter.

Chapter 3

Thermal Zone Modeling

The system dynamic of zone $i \in \{1, \cdots, n\}$ can be modeled using the differential equation

$$\begin{aligned} c_i \frac{dT_{z,i}(t)}{dt} &= u_i(t) + v_i(t) + w_i(t) + q_i(t) \\ u_i(t) &= \dot{m}_i c_p \left(T_{d,i}(t) - T_{z,i}(t)\right) \\ v_i(t) &= \sum_{j \in \mathcal{A}_i} a_{i,j}(T_{z,j}(t) - T_{z,i}(t)) \\ w_i(t) &= b_i(T_o(t) - T_{z,i}(t)) \end{aligned} \tag{3.0.1}$$

where $T_{z,i}[^\circ\text{C}]$ is the temperature of zone i; $u_i[\text{kW}]$ is the HVAC heating input (negative value means cooling input); $v_i, w_i[\text{kW}]$ are the heat transfer from adjacent zones and outside space via envelops; $q_i[\text{kW}]$ is the thermal load on zone i due to the internal heat gain (e.g. occupants, lighting, equipments), transmitted solar radiation, and other untraceable disturbances; $\dot{m}_i[\text{kg/s}]$ and $T_{d,i}[^\circ\text{C}]$ are the discharge air mass flow rate and temperature, respectively; $T_o[^\circ\text{C}]$ is the outside air temperature; $\mathcal{A}_i$ is the index set which contains all the zones that are adjacent to zone i; The constant $c_p[\text{kJ/(kg}^\circ\text{C)}]$ is the specific heat capacity of air, $c_i[\text{kJ/}^\circ\text{C}]$ is thermal mass of the i-th zone, $a_{i,j}, b_i[\text{kW/}^\circ\text{C}]$ are the thermal conductivities between zone i and adjacent space (zone j and outside).

The system dynamics are generally nonlinear as in equation (2.2.7). The model (3.0.1) is assumed to be a linearized model around its nominal operating conditions. Furthermore, the discrete time system model need to be derived in order to design and implement the direct digital control.

The discrete time system model is obtained by Euler forward discretization with sampling time Δt

$$T_{z,i}(k+1) = A_i T_{z,i}(k) + B_i(u_i(k) + v_i(k) + w_i(k) + q_i(k)) \tag{3.0.2}$$

where k is the time step. The effect of different discretization methods was studied in [41].

3.1 Simulation based identification

Building simulation, which is also called energy modeling, has come a long way in the last ten years with the development of computer technology. There are stricter code compliance regulations such as Title 24 [18] and voluntary rating systems like LEED rating systems [42] requesting a performance based simulation approach. This modeling method is preferable when evaluating different design features and retrofitting efficiency measures across the entire building lifecycle. It requests the building geometry construction, envelope and facade design, material property specification, building equipment design (e.g., HVAC and lighting), plug and process load estimation, and programmatic and operational parameters assignment.

The simulation engine ables to provide relatively accurate energy estimation for new construction with an accuracy of +/5% and for existing buildings with parameters calibration [43].The Building Resistance-Capacitance Modeling (BRCM) Matlab Toolbox [44] provides a means for the generation of linear models from basic geometry, construction and building systems data. It decomposed the full model into a thermal model of the building structure (3.1.1) and several external heat flux (EHF) models (3.1.2).

$$\dot{x} = A_t x(t) + B_t q(x(t), u(t), v(t)) \tag{3.1.1}$$

$$q(x(t), u(t), v(t)) = A_q x(t) + B_{q,u} u(t) + B_{q,v} v(t) + \sum_{j=1}^{n_u} (B_{q,vu,j} v(t) + B_{q,xu,j} x(t)) u_j(t) \tag{3.1.2}$$

where x denotes the states (temperatures of zone or building elements), u denotes the input (discharge air mass flow rate for each zone), and v the disturbances (outside air temperature, supply air temperature, solar radiation, etc.).

The thermal model input data contain information about zones and building elements (wall/floor/ceiling/roof), including adjacent connections, windows, constructions and materials. It can be obtained directly from EnergyPlus input data file by parsing objects from certain classes. It is so far the most convenient semi-automated way compared to purely user-specified, although the conversion algorithm has some limitations, for example no doors and internal windows are allowed, and window properties have to be modified by hand. Figure 3.1 shows the target building's ge-

ometry, note that the unified and aggregated result after conversion (e.g. at most one window per building element is allowed).

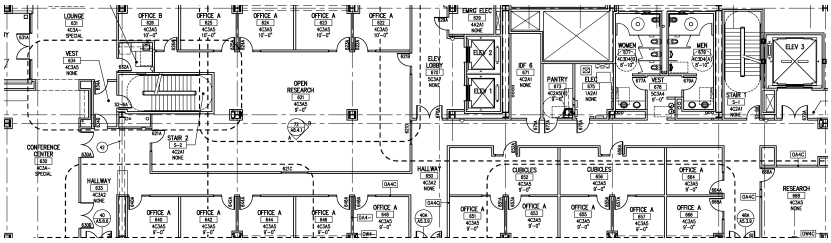

(a) Floor plan

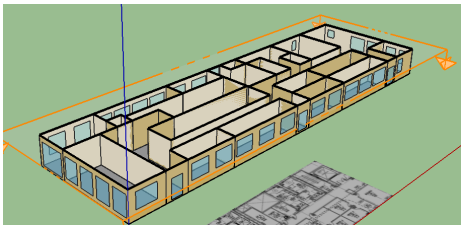

(b) Building geometry in SketchUp

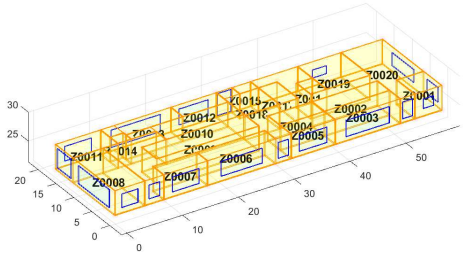

(c) Aggregated building geometry in BRCM

Figure 3.1: Geometry of the studied building (5th floor, Sutardja Dai Hall)

The system matrices A_t, B_t, A_q, B_q are functions of tuning parameters: the window heat transmission coefficient, the convection coefficients of interior wall, exterior wall, floor, and the ceiling. Those parameters can be identified using optimization such that the difference between the measured temperature and the simulated temperatures is minimized. More detail work can be found in [44] and [45]. It is worth noting that the system states are not all measurable, therefore state estimation method such as Kalman Filter must be implemented in conjunction with control algorithm. Figure 3.2 plots the validation results over a week period. One can observe that the prediction match well with the actual measurement.

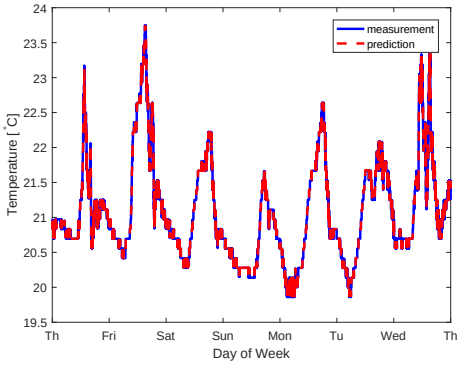

(a) Testing result of the zone temperature

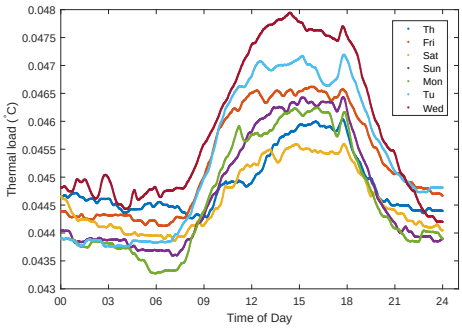

(b) Estimation of the thermal load

Figure 3.2: Validation result of BRCM model

3.2 Data-driven based identification

In this section, we used the Simple Measurement and Actuation Profile (sMap) [46] database[1] from Sutardja Dai Hall as our data source for training our thermodynamics model. All collected data are down-sampled or interpolated to 15 minute intervals.

To be specific, two rooms are chosen to be studied: Bechtel Board Room (Room 630) is a peripheral conference room with large windows, and Chan Room (Room 240) is an interior classroom without any window, as shown in Figure 3.3.

Generally speaking, model identification is usually more accurate when the control inputs are independent of the system states or external input. However, since most of the buildings nowadays have already been equipped with some decent and similar control system and doing extra forced response experiments might disturb the occupancy comfort, the data used in this project is from normal operation.

Semiparametric model

The semi-parametric regression method to identify a partially linear model was proposed in [47]. Consider a simple discrete thermal model for single zone

$$T(k+1) = aT(k) + bu(k) + cv(k) + q(k) + \epsilon(k) \tag{3.2.1}$$

where a, b, c are some time constants related to the room inherent time-invariant physics properties, T is the room temperature, u is the VAV box heating input, v is

[1] `http://www.openbms.org/dashboard/`

(a) Conference room

(b) Classroom

Figure 3.3: Two examples for model identification.

the outside air temperature, and q is the change in temperature due to intractable disturbance, such as solar radiation and internal heat gain due to occupancy activity and equipment in the room. In addition, ϵ is assumed to be independent and identically distributed zero mean noise with constant variance.

We take the conditional expectations on both sides of (3.2.1) to get

$$\mathbb{E}\left[T(k+1)|k+1\right] = a\mathbb{E}\left[T(k)|k\right] + b\mathbb{E}\left[u(k)|k\right] + c\mathbb{E}\left[v(k)|k\right] + \mathbb{E}\left[q(k)|k\right] + \mathbb{E}\left[\epsilon(k)|k\right] \tag{3.2.2}$$

Take the temperature variable $T(k)$ for example, if we can find an estimator $\hat{T}(k)$ to estimate the conditional expectation $\mathbb{E}\left[T(k)|k\right]$, then we can further write (3.2.2) into

$$\hat{T}(k+1) = a\hat{T}(k) + b\hat{y}(k) + c\hat{v}(k) + \mathbb{E}\left[q(k)|k\right] + \mathbb{E}\left[\epsilon(k)|k\right] \tag{3.2.3}$$

Noting that and $\mathbb{E}\left[q(k)|k\right] = q(k)$ and $\mathbb{E}\left[\epsilon(k)|k\right] = 0$, so subtracting (3.2.3) from (3.2.1) gives

$$T(k+1) - \hat{T}(k+1) = a(T(k) - \hat{T}(k)) + b(u(k) - \hat{y}(k)) + c(v(k) - \hat{v}(k)) + \epsilon(k) \tag{3.2.4}$$

The key highlight of this method is that the unknown disturbance $q(k)$ term has been eliminated, and thus the parameters a, b, c can be estimated using any regression method, such as regularized least square.

$$\begin{aligned} \min_{a,b,c} \sum_{k} \big(T(k+1) - \hat{T}(k+1) - a(T(k) - \hat{T}(k)) \\ - b(u(k) - \hat{y}(k)) - c(v(k) - \hat{v}(k))\big) + \lambda\|(a,b,c)\|^2 \end{aligned} \tag{3.2.5}$$

Further, with the estimated coefficients $\hat{a}, \hat{b}, \hat{c}$, the unknown disturbance can be estimated by manipulating (3.2.3)

$$\hat{q}(k) = \hat{T}(k+1) - \left(\hat{a}\hat{T}(k) + \hat{b}\hat{u}(k) + \hat{c}\hat{v}(k)\right) \tag{3.2.6}$$

There is one last but not least concerning about how the estimators are computed. According to [47], there are a variety of estimators which are equivalent to smoothing over time. We argue that the choice of estimator will give dramatically different results.

Nadaraya-Watson kernel regression In any nonparametric regression, the conditional expectation of variable X relative to time index k can be written as a locally weighted average, using a kernel as a weighting function. The Nadaraya-Watson estimator is

$$\hat{X}(k) = \frac{\sum_{i=1}^{m} K(k-k_i)X_i}{\sum_{i=1}^{m} K(k-k_i)} \tag{3.2.7}$$

where K is a kernel with some bandwidth. The optimal set of parameters is $(\hat{a}, \hat{b}, \hat{c}) = (0.60, 0.27, 0.02)$. The estimated disturbance calculated with (3.2.6) is shown in Figure 3.4a.

Locally weighted smoothing (LOWESS) regression For standard locally weighted linear regression with a tri-cube weight function, we can use $k-$fold cross-validation to determine the bandwidth.

The optimal set of parameters is $(\hat{a}, \hat{b}, \hat{c}) = (0.18, 0.32, 0.01)$. The estimated disturbance calculated with (3.2.6) is shown in Figure 3.4b.

This method separates the thermal model terms and the unknown disturbance term in the statistical sense. The estimator can be viewed as a small deviation from the measurement value, thus this method can only work when there is enough difference between the estimator and the measurement value, i.e. the variable values have been changed during the operation time. If there is not sufficient excitation, the temperature will not change much, the optimal parameter set will be all zeros.

Even if there is enough variation in the temperature, we can get completely different models using different estimators. This is an evidence to show that the model we obtained using this method cannot be trusted for control design. The estimated disturbance can also be different in the scale of $10°C$ as shown in Figure 3.4.

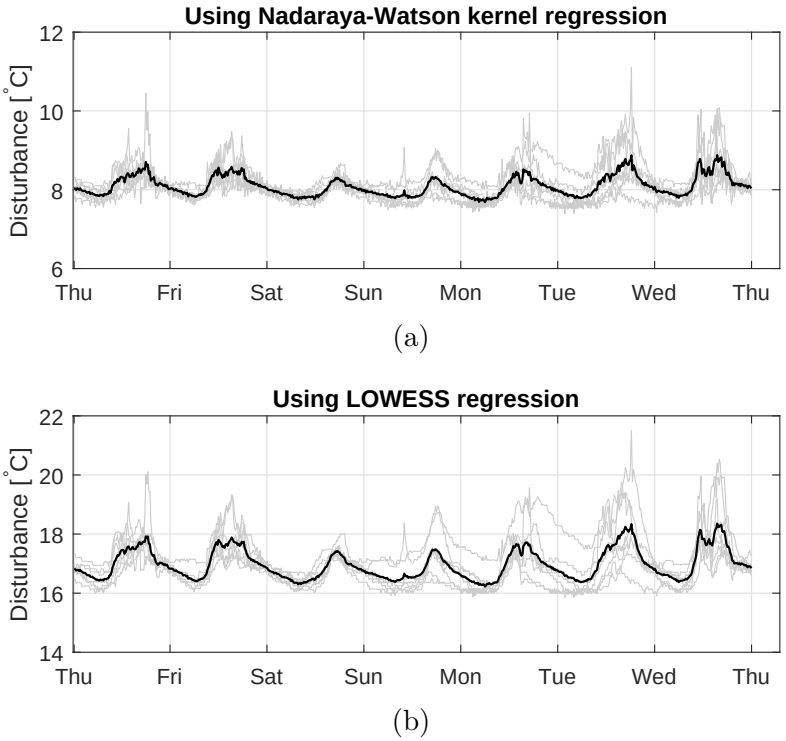

Figure 3.4: The estimated disturbance. Gray lines are for individual weeks in the training set, black line is the average.

Another thing to be noted that the open-loop predictions of the temperature using the average weekly disturbance estimator are not good, as shown in Figure 3.5. The root mean square errors of prediction are 0.49 and 0.5 respectively.

Polynomial model

It is usually either hard or expensive to capture accurately the internal heat gains from human activities. As a result, we used the data collected over the weekends for training our models to circumvent those uncertainties, as is done by other reported approaches in literature [47, 48]. The reason for also including the daytime data besides the nighttime data in our training set is because there is usually a lack of excitation during the night for accurate identification of the thermodynamics; however, we will then also need a way to decouple the excitation from solar radiation

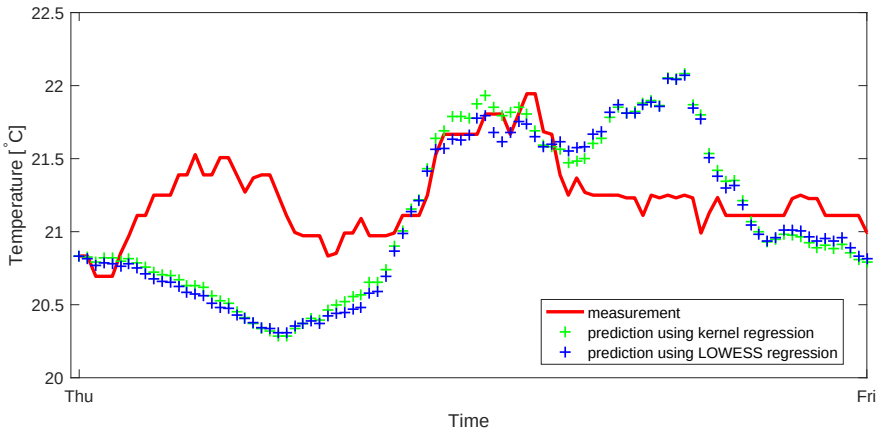

Figure 3.5: The open-loop prediction using average disturbance function.

from other sources.

In our approach, the unknown solar radiation in the thermodynamics is modeled as an additional posynomial/polynomial disturbance term

$$q_{\text{solar}} = \sum_i x_i \left(\prod_{j=1}^{n} w_j^{\alpha_{ij}} \right) = \sum_i x_i w^{\alpha_i} = \sum_i \phi_i x_i = \Phi x, \tag{3.2.8}$$

where $w_1, w_2, \ldots, w_n$ are the features for the monomial term, and $\alpha_i = \{\alpha_{ij}\}$ is one particular choice of the exponents for each feature w_j. $\phi_i = w^{\alpha_i}$ (component-wise exponent operation) is the ith column of Φ.

In order to decouple the effects of q_{solar} on the zone temperature from other inputs to the thermodynamics equation, it will be helpful to incorporate some prior knowledge on the time frame that q_{solar} exists. To do that, we introduce a time-varying multiplier $\eta(k)$ modeling the "active window" of the solar radiation using a combination of two sigmoidal membership functions as shown in Figure 3.6. The parameters in (3.2.9) are chosen as above such that $\eta(k) > 0.5$ between 11AM and 6PM, which is roughly the time frame that the west-facing experimental zone will receive direct sunlight.

$$\eta(k) = \begin{cases} f_s(x, 1/30, 11 \times 60), & 0 < H(k) \leq 14 \\ 1 - f_s(x, 1/30, 18 \times 60), & 14 < H(k) \leq 24, \end{cases} \tag{3.2.9}$$

$$\text{where } f_s(x, a, c) = \frac{1}{1 + e^{-a(x-c)}}. \tag{3.2.10}$$

By multiplying $\eta(k)$ to the features we used to fit the polynomial solar radiation model, we can ensure solar radiation is close to zero outside the active window. It is worthy to note that, in this approach, no prior assumption on the relative magnitude of the solar radiation within its active window has been imposed.

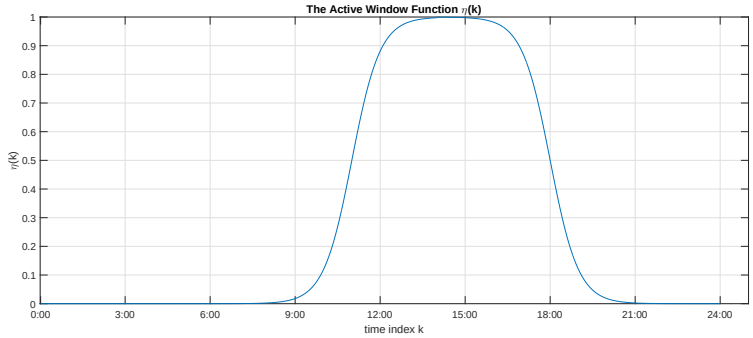

Figure 3.6: The active window function $\eta(k)$ over the span of a day.

In practice, since the posynomial/polynomial model can admit a constant term, we can absorb the constant heat gain in the zone into the model without any loss of generality. We will denote by q'_{solar} the posynomial/polynomial model representing solar radiation and constant heat gain for the zone.

The objective function to minimize for the sparse posynomial/polynomial identification is of the following form

$$f(b,c,x) = \left\| \begin{pmatrix} bu + cv + \Phi x - y \\ \Sigma \end{pmatrix} \right\|_2 + \lambda_b b + \lambda_c c + \lambda^\top x, \tag{3.2.11}$$

$$= \left\| \tilde{\Phi}' x' - \tilde{y} \right\|_2 + \lambda'^\top x', \tag{3.2.12}$$

where $\Sigma = \sigma I$ is added to regularize Φ in order to improve the numerical condition of the problem (3.2.12). Here, we write the objective in a more compact way by absorbing the terms containing b and c into the posynomial/polynomial term and end up having a LASSO problem, which can be solved either using CVX or coordinate descent methods as to be introduced in the next section. We refer interested readers to the work [49] for a more detailed account on the sparse posynomial/polynomial model identification approach as well as the associating safe feature elimination techniques for speedup.

We have fitted both a posynomial and a polynomial model for the zone we investigated. In the experiment, we set the regularization parameters $\lambda_b = \lambda_c = 0.01$,

Feature	Choice of Exponents	Typical Values
$w_0 = \eta(k)H(k)$	$\{0, 1, 2, 3\}$	0-24
$w_1 = \eta(k)T_{oa}(k)$	$\{0, 1, 2\}$	10-30
$w_2 = \eta(k)T_{oa}(k-4)$	$\{0, 1, 2\}$	10-30
$w_3 = \eta(k)T_{oa}(k-8)$	$\{0, 1, 2\}$	10-30

Table 3.1: Selected Features for the Polynomial Model Training

and all entries in λ to be the same value 0.05. The data collected over four weekend days (Oct 1, Oct 2, Oct 7 and Oct 8 in the year of 2016) are used for training, and the data for another weekend (Sep 17 and Sep 18) in the same season are as the test set. An interval $t_s = 15$min is used in the experiment. To increase the number of data points for the experiment, we pick intervals that have overlaps, e.g. not only the data at the 1st and the 16th minutes, but also the data at the 2nd and 17th minutes, are used as $T(k)$ and $T(k+1)$.

The features we selected to train the posynomial and polynomial models, along with the choices of exponents of each of them, are listed in Table 3.1. The resulting $\tilde{\Phi}$ has 108 columns (i.e. candidate monomials to fit the posynomial/polynomial model). Because the data in each column can be of dramatically different scales, we standardized each column[2] so that they are centered at zero and have a standard deviation of one.

For either model, it took less than a minute on a Intel Core i7 laptop with 8GB memory. The identified thermodynamics using a posynomial model for solar radiation writes

$$\begin{aligned} &y_{\text{posy}}(k) = T(k+1) - T(k) = 0.262 \cdot u(k) + 0.00458 \cdot v(k) + q'_{\text{solar}}, \\ &\text{where} \quad q'_{\text{solar}} = -41.4435 + 2.81 \times 10^{-5} \cdot w_0, \end{aligned} \tag{3.2.13}$$

and it has a Mean Squared Error (MSE) of an MSE of 0.00118 on the training data set and 0.00088 on the test data set.

The identified thermodynamics using a polynomial model (3.2.14), with an MSE of 0.00099 on the training set and 0.00092 on the test set, have many more terms compared to the one above. The error distributions for both models on the training

[2]By using `zscore` function in MATLAB

and test data are given as histograms in Figure 3.7.

$$
\begin{aligned}
&y_{\text{poly}}(k) = T(k+1) - T(k) = 0.311 \cdot u(k) + 0.00716 \cdot v(k) + q'_{\text{solar}},\\
&\text{where } \; q'_{\text{solar}} = -41.46 + 4.3 \times 10^{-3} \cdot w_3 - 1.64 \times 10^{-6} \cdot w_2 w_3\\
&- 2.31 \times 10^{-8} \cdot w_1 w_2 w_3 + 1.37 \times 10^{-6} \cdot w_1 w_2 + 1.96 \times 10^{-3} \cdot w_0 w_3\\
&- 0.0021128 \cdot w_0 w_1 - 8.13 \times 10^{-7} \cdot w_0 + 7.1698 \times 10^{-8} \cdot w_0 w_3\\
&+ 2.4357 \times 10^{-7} \cdot w_0 w_2 - 3.39 \times 10^{-6} \cdot w_0 w_1. \qquad (3.2.14)
\end{aligned}
$$

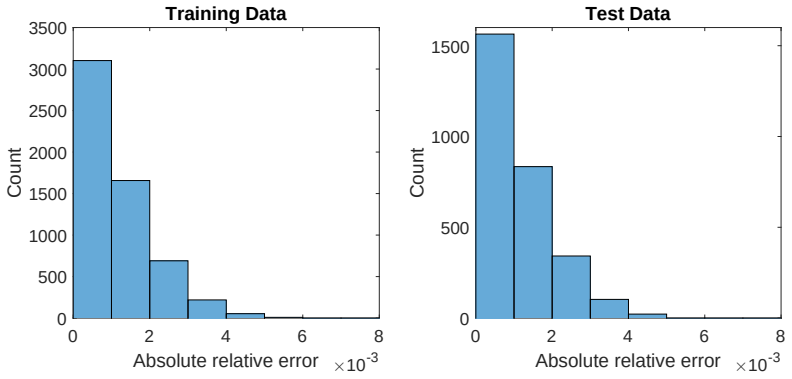

(a) Posynomial Model

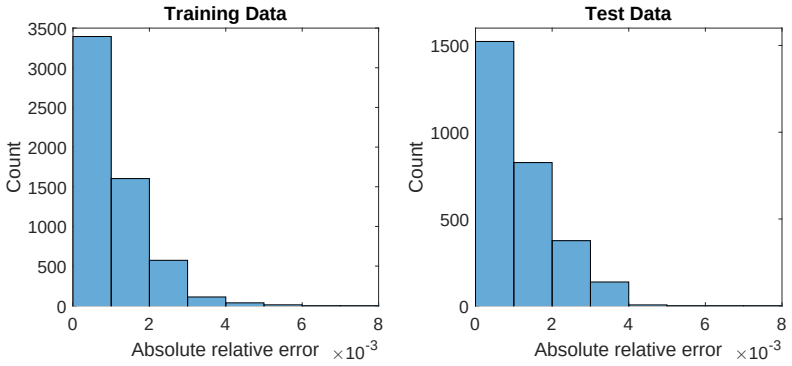

(b) Polynomial Model

Figure 3.7: Histograms showing the error distribution on the training data and the test data sets.

To detail how each component in the identified thermodynamics equations (3.2.13)(3.2.14) contributes to the fitted model, we plot the prediction of $bu(k)$, $cv(k)$ and $q'_{\text{solar}}(k)$

over the test period, respectively in Figure 3.8 and in Figure 3.9 for the posynomial and the polynomial model. As we can see from both models, the solar radiation prediction reaches it maximum at around 4.30 pm, which matches the physics since the windows in the zone is facing westwards. We further do an experiment to see

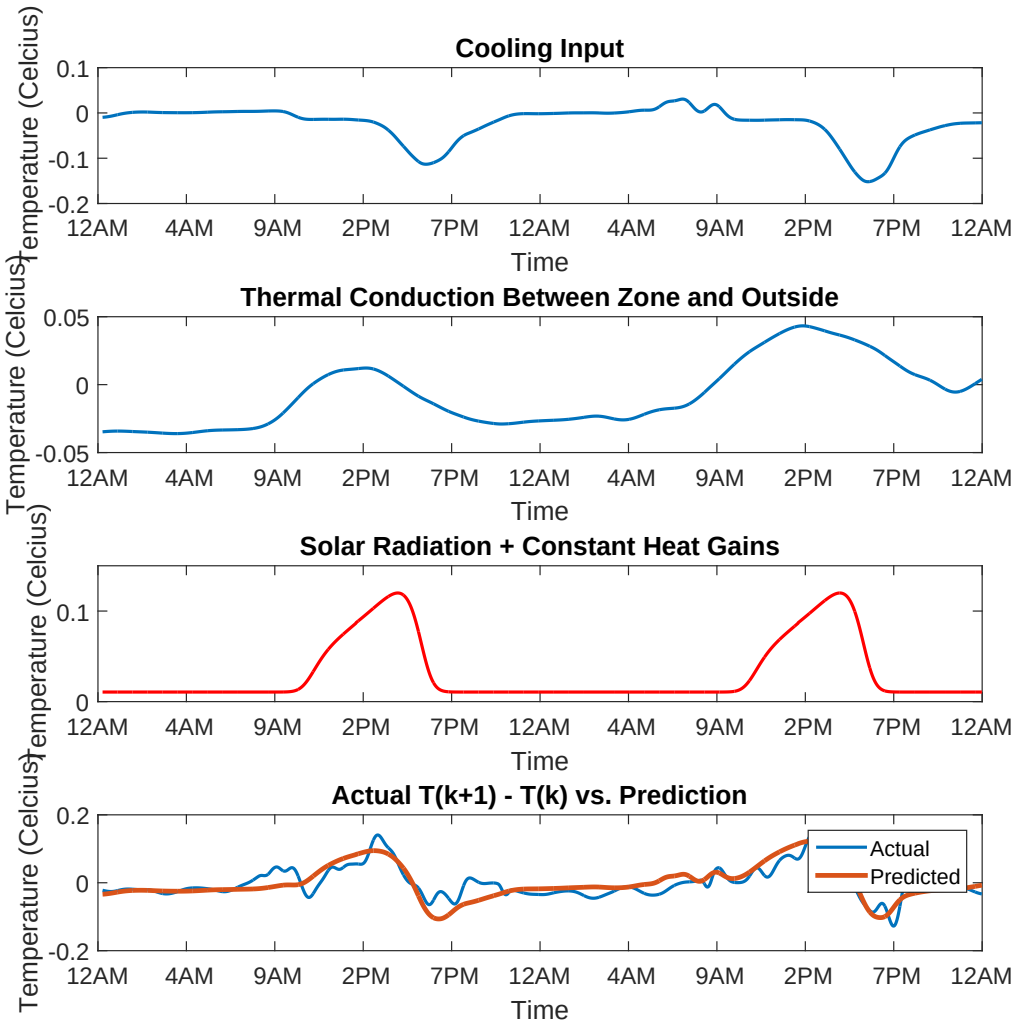

Figure 3.8: A breakdown of the identified posynomial model that shows how each term contributes to the fitted $y_{\text{posy}}(k)$.

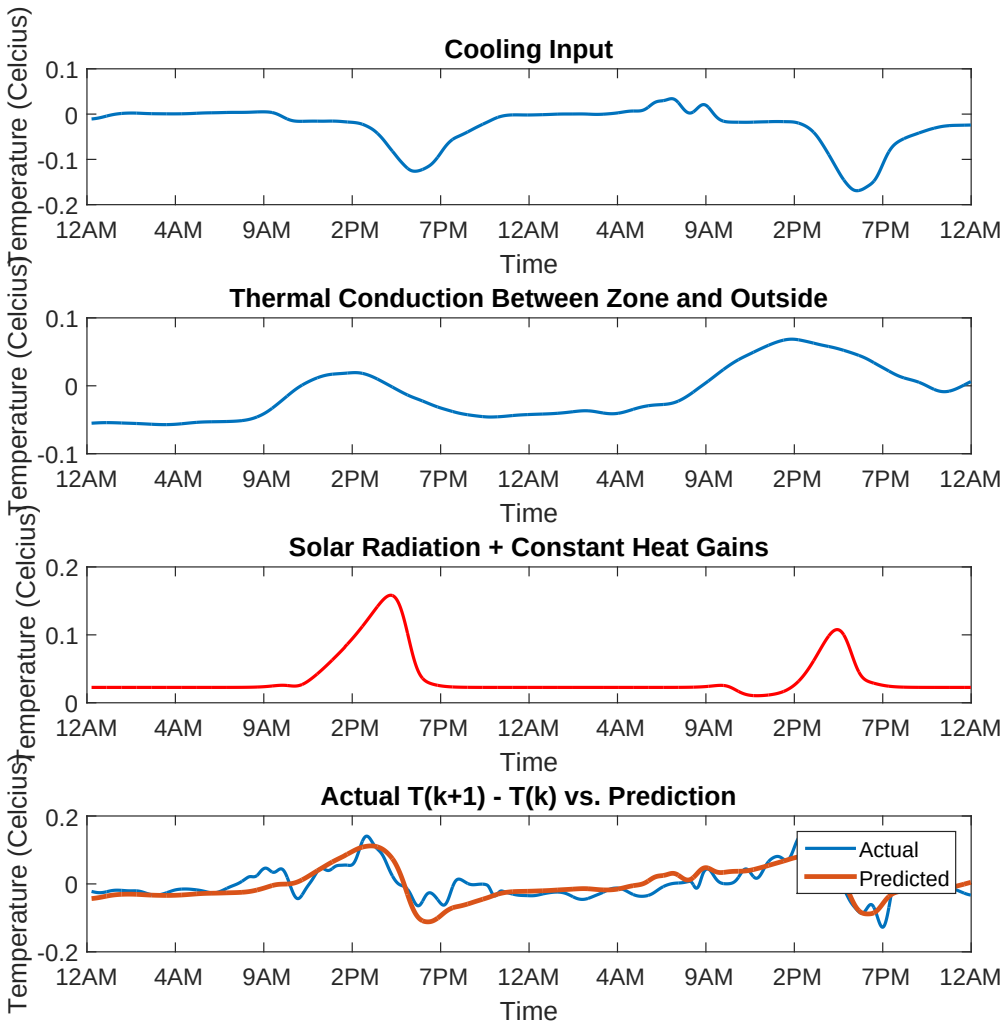

Figure 3.9: A breakdown of the identified polynomial model that shows how each term contributes to the fitted $y_{\text{poly}}(k)$.

how the identified model with solar radiation estimate performs in an open-loop prediction. The results for both models are shown in Figure 3.10. It can be seen again that the prediction accuracy of both models are similar, although the polynomial model has many more terms than the posynomial one.

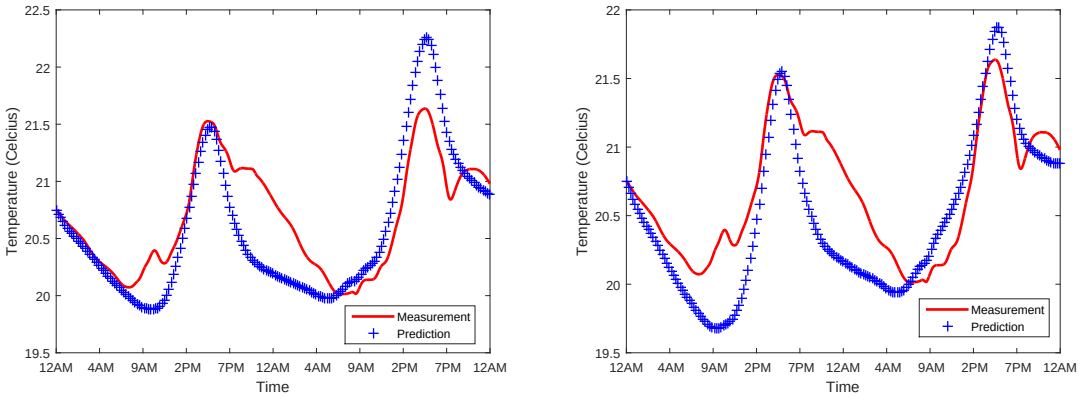

(a) Posynomial Model (b) Polynomial Model

Figure 3.10: Open-loop prediction results of both models on the test data set.

Slow Feature Analysis (SFA)

The model of temperature dynamics can be reasonably approximated as first-order difference equation as follow

$$T_z(k+1) = aT_z(k) + bu(k) + q(k) \tag{3.2.15}$$

where q is the total thermal load on zone i due to the net heat gain through envelop, internal heat gain (e.g. occupants, lighting, equipments), solar radiation, and other untraceable disturbances.

Standard parameter identification techniques cannot be used since $q(k)$ is unknown and is expected to be highly nonlinear with respect to time. Section 3.2 uses conditional expectations to eliminate the uncertain disturbance term, while section 3.2 parametrizes $q(k)$ with a polynomial basis, and then identify all parameters using nonlinear regression. An unsupervised learning algorithm which is robust and fast, called SFA [50], is adopted here to estimate the thermal load. It has been successfully applied to signal processing, such as invariant object recognition and gesture recognition.

Given multidimensional time-varying input signals, $\{x(k)\}$, SFA can instantaneously generate slowly-varying output signal, $\{y(k)\}$, by searching different nonlinear combinations of the input signals.

$$\min\langle\dot{\bar{y}}^2\rangle \text{ s.t. } \langle\bar{y}\rangle = 0, \langle\bar{y}^2\rangle = 1, \bar{y} = g(x(k)) \tag{3.2.16}$$

where the bracket $\langle\cdot\rangle$ indicates the temporal mean. To avoid the trivial constant solution, we need to add constraints of zero mean and unit variance.

In this application, we choose $\{T_z(k), T_o(k), \dot{m}(k), T_d(k), U(k)\}$ as the input time series, and other choices or combinations are also acceptable. Note that SFA can only give a normalized $\{\bar{q}(k)\}$ time series with zero temporal mean and unit variance, the scale and offset factors related to the true value are fixed and need to be identified as well. Then, the parameter identification problem is formulated as

$$(\hat{a}, \hat{b}, \hat{c}, \hat{d}) = \arg\min_{a,b,c,d} \|T_z(k+1) - aT_z(k) - bU(k) - c\bar{q}(k) - d\|^2 \tag{3.2.17}$$

With the estimated parameters in hand, the estimation of thermal load can be estimated as

$$\hat{q}(k) = \hat{c}\bar{q} + \hat{d} \approx T_z(k+1) - \hat{a}T_z(k) - \hat{b}u(k) \tag{3.2.18}$$

The results for two case studies are shown in Figure 3.11 and Figure 3.12. The interesting observation is that internal heat gain due to occupants is much less than the solar radiation and heat gain from outside air through windows. The base load is high for the conference room is because of the large thermal mass of the peripheral walls. The wall has been heated during the day and behave as a heat sink at night.

The model advocated here is particularly attractive when the fine-grained measurement data is available, and detail floor plan or structural characteristics are unknown.

3.3 Summary

In this chapter, the different approaches for building thermal dynamic modeling are presented. The simulation-based approach needs extra effort to model the geometry and construct state estimators to estimate the unmeasurable variables. While the data-driven based approaches achieve a balance between the model complexity and model accuracy. However, the identification and estimation results subject to training data and might yield unphysical predictions.

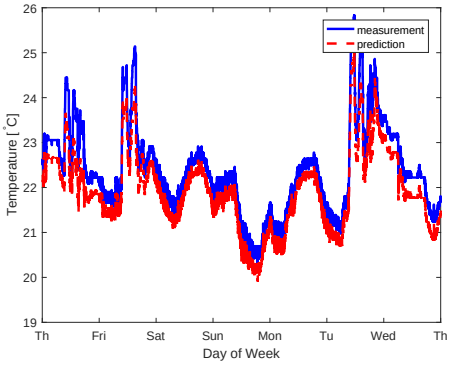

(a) Testing result of the zone temperature

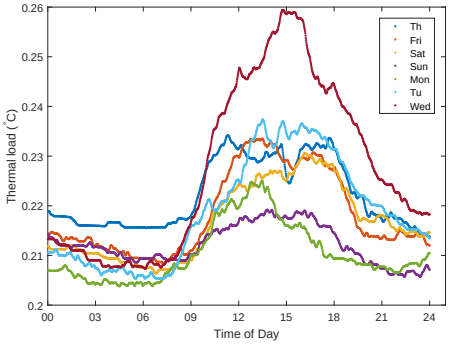

(b) Estimation of the thermal load

Figure 3.11: Validation result of SFA model - conference room

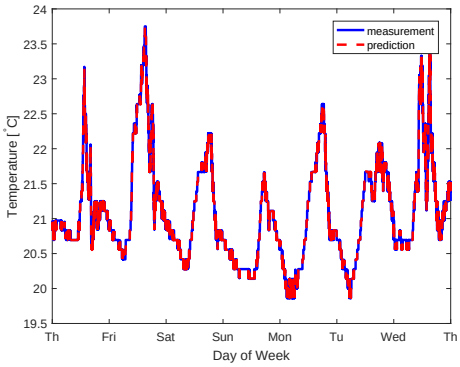

(a) Testing result of the zone temperature

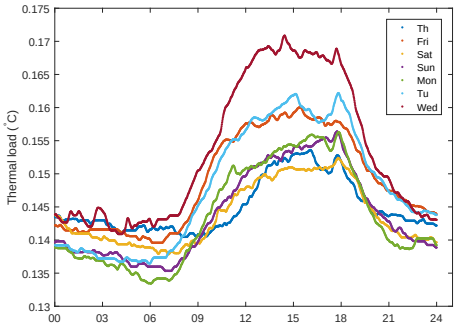

(b) Estimation of the thermal load

Figure 3.12: Validation result of SFA model - classroom

Chapter 4

Optimal Control Design

The optimal control design of energy efficient HVAC system can be casted into an optimization problem 4.0.1: the optimal goal is to minimize the total utility cost, while subject to system models and comfort constraints, as well as physical constraints as described in Chapter 2.

$$\begin{aligned} \min_{\boldsymbol{u}_k} \quad & \sum_{k=0}^{N-1} C(\boldsymbol{u}_k) \\ \text{subject to} \quad & \forall k = 0, \cdots, N-1 \\ & \boldsymbol{x}_{k+1} = f(\boldsymbol{x}_k, \boldsymbol{u}_k, \boldsymbol{v}_k, \boldsymbol{w}_k) \\ & \underline{\boldsymbol{x}}_{k+1} \leq \boldsymbol{x}_{k+1} \leq \overline{\boldsymbol{x}}_{k+1} \\ & \underline{\boldsymbol{u}} \leq \boldsymbol{u}_k \leq \overline{\boldsymbol{u}} \end{aligned} \tag{4.0.1}$$

$\boldsymbol{x}_k$	Zone temperatures
$\boldsymbol{u}_k$	Controllable set-points, e.g. T_s, $\dot{\boldsymbol{m}}$, $\boldsymbol{T}_d$
$\boldsymbol{v}_k$	Measured disturbances, e.g. solar radiation, weather
$\boldsymbol{w}_k$	Unknown disturbances, e.g. internal heat gain

4.1 Current industry best practice

Dual-maximum control [13]

Modern VAVs use a feedback controller to adjust the rate and temperature of airflow supplied to each thermal zone according to changes in cooling and heating load in order to maintain occupant thermal comfort. The two predominant control logics in existing VAVs are single-maximum and dual-maximum as shown in Figure

4.1. The cooling and heating loop are intermediate control numbers, in percentage between 0 and 100%, which are the outputs of PI control of zone temperature. There is a specific comfort temperature range bounded by the heating and cooling setpoint, $\mathcal{T} = [\underline{T_z}, \overline{T_z}]$, which is also called dead band since the zone does not require any heating or cooling within the range. Then the loop responses are determined by the deviation between the zone temperature and the two setpoints. The minimum airflow setpoint is suggested to be either the minimum ventilation requirements for sufficient fresh air mixing, or the smallest controllable airflow allowed by the damper (from both accuracy and stability perspective), whichever is larger.

The single-maximum control logic is programmed to provide maximum airflow at the design cooling condition and gradually drop discharge airflow to the minimum airflow setpoint, which is often set by the airflow required at the design heating condition, as cooling load decreases. The hot water valve position is controlled linear with heating loop. While the dual-maximum control logic increases airflow in heating mode once the heating loop exceeds a certain number to prevent air stratification issues, which results two maximum airflow setpoints. And the discharge air temperature set directly instead of the hot water valve. Compared with single-maximum logic, dual-maximum control logic allows for much lower minimum airflow, (e.g. 10-20% vs 30-50% of maximum of heating airflow), and thus lower energy consumption of heating, cooling and fan. Building code and energy standards Title 24[18], ASHRAE 90.1[17] require implementing or retrofitting to dual-maximum control logic for new or existing construction respectively.

The control logics is just piece-wise linear with respect to the cooling and heating loopout, which is the PID output of the zone temperature.

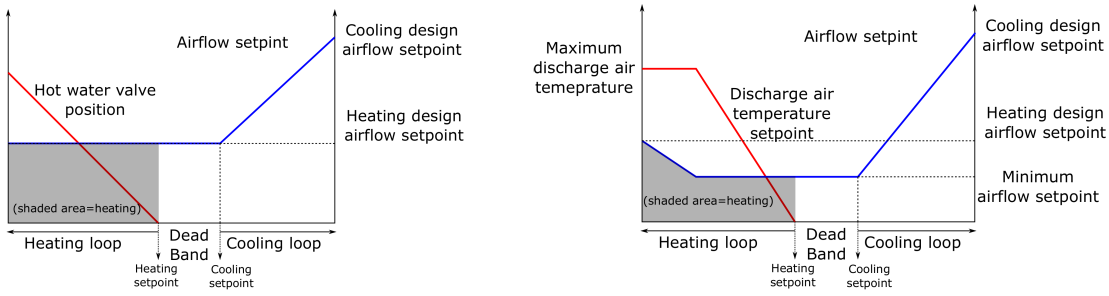

(a) Single-maximum (b) Dual-maximum

Figure 4.1: Industrial VAV practice control logic

Trim and Respond[10]

The Trim and Respond logic is advocated by many compliance building codes and standards. It is also called demand-based reset since the setpoints vary based on the requirement of the most demanding ("critical") zone.

Duct static pressure reset The duct static pressure should be just high enough so that the most demanding VAV terminal unit in the building (the critical unit) has sufficient pressure to meet its current airflow setpoint. This control strategy is known as a duct static pressure reset, and it is required by both ASHRAE 90.1 [17] and California Title 24 [18]. It is typically achieved by resetting the duct static pressure setpoint upwards when a zone requests increased pressure (typically when a VAV damper is nearly wide open and the airflow is still below the maximum airflow setpoint), and allowing the setpoint to slowly decrease when there are no requests. This reduces static pressure (and fan power) to the minimum needed to meet the current airflow requirements for all of the zones in the building, and can generate fan energy savings from 30-50% compared to fixed duct static pressure setpoints [51]. Typically, there is also a user-defined number of requests that will be ignored, particularly in systems with many zones, as one faulty (rogue) zone would otherwise drive the entire reset strategy.

Supply air temperature (SAT) reset Similarly, the SAT should be controlled using a SAT reset strategy, so that the most demanding VAV terminal unit receives supply air that is just cool enough to meet its zone cooling temperature setpoint, as defined by the thermal comfort requirements for that zone. This is typically achieved by resetting the SAT setpoint downwards when a zone requests cooler air, and allowing the setpoint to slowly increase when there are no requests. As for the duct static pressure reset, there is also a user-defined number of requests that are ignored. SAT reset is currently prescriptively required in Title 24 and Standard 90.1 but the requirements allow the reset to be in response to representative building loads or simply to outdoor air temperature SAT reset based on outdoor air temperature is a common approach in systems without feedback from the individual zone, but it has a significant drawback in that it is an open loop feedback strategy that runs the risk of not maintaining comfort and not realizing maximum energy savings.

However, unlike a duct static pressure reset where lower values always provide energy savings, there is an additional consideration in the case of SAT reset: the potential to save energy by supplying lower temperature air while still meeting comfort conditions in the zones in the building. Reducing the SAT setpoint beyond the point at which comfort needs are met has three primary effects:

1) It reduces the airflow required by any zones that are currently in cooling mode, which reduces fan energy consumption in a cubic relationship with respect to airflow

2) It increases the reheat energy used in any zones that are currently in heating mode, in a linear relationship to temperature

3) It will increase cooling energy at the AHU depending on the status of the economizer, i.e., if the outside air temperature is higher than the SAT.

4.2 Cost-responsive supply air temperature reset strategy

Existing SAT reset strategies make inherent simplifications and assumptions about the relationship between SAT and total HVAC energy cost. As industry best practice has progressed from a fixed setpoint; to a setpoint that varies based solely on outside air temperature; to the warmest possible setpoint that will still provide comfortable conditions based on feedback from every zone; to a combination of the last two approaches (current practice) there has been an inherent assumption that each new strategy has improved overall energy efficiency. However, none of these approaches will find optimum SAT under all operating conditions, as that optimum value depends on a wider range of conditions in the building than simply the current outside air temperature and SAT. Furthermore, the first two strategies do not incorporate feedback from the zone, and thus had an additional issue - they do not guarantee that comfort conditions will be met in all zones in the building.

It can be viewed as a hybrid system approach by forcing the supply air temperature setpoint to belong to a finite set of values, i.e. $T_s^{sp} \in \mathcal{M} = \{T_{s,1}^{sp}, \cdots, T_{s,p}^{sp}\}$, where p is the number of modes. The new strategy dynamically estimates the total HVAC energy cost at a particular SAT setpoint, and then iteratively moves in the direction of least cost, while subject to the same constraint to maintain comfort conditions as the current industry best practice [52].

We strove to reduce complexity to a minimum to ensure that this approach is feasible to implement at scale within the building automation systems currently in use today. Similarly, to ensure that this could be implemented cost effectively, we also constrained the required measurements to a minimum set of data that are likely already present in a modern VAV system. We assume direct digital controls (DDC) to each zone, with an airflow measurement at each VAV terminal unit, and a zone discharge air temperature measurement after each reheat coil. At the AHU, we as-

sume that there is a mixed air and supply air temperature measurement and a power output from the variable frequency drive. These are all very common measurements in a modern VAV system, many of which are requirements in codes and standards.

A high-level overview of the proposed control strategy is as follows. At each (user-defined) time interval (typically 5 minutes), we compare the estimated HVAC energy cost at the current SAT setpoint with the estimated costs at alternative SAT setpoint values. We then adjust the setpoint to the lowest cost value and repeat the process at the next time interval. This strategy assumes that the energy and cost estimates are reasonably accurate, and the estimated value corresponds to the steady state power consumption of the system.

In our implementation, we first determine a vector of fixed temperature differences, ΔT_s, e.g. $[-0.6°C, -0.3°C, 0°C, 0.3°C, 0.6°C]$. We use these to calculate a vector of candidate SAT setpoints within the feasible range of setpoint values. For example, if the current SAT setpoint is $11.8°C$ and the feasible range of SAT setpoints is $11.7°C$ to $18.3°C$, then we calculate the candidate setpoints using the temperature difference vector, ensuring that the lowest and highest values remain within the feasible range: $[11.7°C, 11.7°C, 11.8°C, 12.1°C, 12.6°C]$. At each iteration, we select the best candidate based on a cost estimation method that we describe in the next section.

In addition, cooling requests from zones take priority over the energy cost signals to ensure comfort requirements are met. If the number of zone cooling requests exceeds a user-defined number to ignore (e.g. 9 rooms in the building request more cooling while the threshold to ignore is 8), we default to the standard trim and respond logic to ensure that the VAV system meets comfort needs in the building in the same manner as current industry best practice meets those needs. However, the range of feasible setpoints in which the trim and respond logic can operate is not constrained by the outside air temperature limits used in the current best practice logic.

In case an exception or error occurs during the computation, the program falls back to the current industry best practice trim & respond strategy, and if an exception occurs there, the program writes a reasonable fixed default setpoint value.

Airflow and fan power model

We estimate the change in fan power change according to the candidate SAT setpoint values by first estimating each zone air flow rate at the new SAT, determining the new system airflow rate based on the sum of zones, and then calculating the fan power at that new airflow rate.

When a zone is not in cooling mode, or when it is making a cooling request, the zone airflow estimate is the same for all candidate SAT setpoints - the zone minimum airflow setpoint or zone maximum airflow setpoint respectively. Where a zone is in cooling mode, the airflow estimate is:

$$\hat{V}_i(k+1) = V_i(k) \left(\bar{T}_i(k) - T_{d,i}(k)\right) / \left[\bar{T}_i(k) - (T_{d,i}(k) + \Delta T_s)\right] \tag{4.2.1}$$

where $V_i(k) = \dot{m}_i(k)$, $\bar{T}_i(k)$ is the temperature cooling setpoint. There are accuracy concerns with these simplifications, as there are for the other estimation methods. When the zone temperature is just below the zone cooling setpoint, the zone will not be in cooling mode and the zone airflow estimate will remain at the zone minimum airflow setpoint. Clearly, moving to a candidate SAT that is higher than the current SAT will cause the zone to enter cooling mode, and the airflow will increase. This state change effect is not captured by this estimation method. However, it will be captured after a subsequent iteration of the controller - once the SAT moves to the new candidate setpoint, and the zone enters cooling mode. Also, this approach applies to zones that use either single-max or dual-max logic at the VAV box. Even with dual-max sequences, when the airflow increases in the second stage of heating, that airflow increase is independent of the supply air temperature it occurs at a fixed discharge air temperature setpoint.

Finally, we use the airflow estimate and the current airflow to estimate the change in fan power based on the fan affinity law:

$$P_f(k+1) = P_f(k) \left(\frac{\sum \hat{V}_i(k+1)}{\sum V_i(k+1)} \right)^3 \tag{4.2.2}$$

Coil power model

The heating and cooling coils are air-water heat exchangers. In a simple coil model, we compute the instantaneous power used in a coil as the product of the air flow measured across the coil and the temperature difference between the inlet and outlet air. Note that there will be a temperature change across the coil when the valve is closed whether it is a coil in the air handling unit or a coil in a terminal unit. This temperature change can be caused by a combination of duct heat gain (or loss), a passing valve, fan heat gain, thermal capacitance of the coil and fluid in the coil, and/or measurement error. We estimate this temperature difference, i.e. T, using the inlet and outlet temperature when the valve has been closed for an extended period (the default is 5 minutes). This time period is long enough for the fluid in the coil to approach steady state temperature with the air. In this way, we

dynamically calibrate the temperature sensor pair so that we only estimate the heat transfer that is intentionally caused by valve operation. We smooth this temperature estimate using an exponential averaging function, where is small (0.001-0.0001) to ensure that the smoothing occurs over a period of days.

The following equations describe the reheat power calculation:

$$\Delta T_{h,i}(k+1) = \begin{cases} \alpha(T_{d,i}(k+1) - T_s(k+1)) + (1-\alpha)\Delta T_{h,i}(k) & \Omega_{h,i}(k) = 0 \\ \Delta T_{h,i}(k) & \Omega_{h,i}(k) > 0 \end{cases} \tag{4.2.3}$$

$$P_h(k+1) = \begin{cases} 0 & \Omega_{h,i}(k) = 0 \\ \sum_{i=1}^{n} \rho c_p \max(0, \hat{V}_i(k)(T_{d,i}(k) - T_s^{sp}(k+1)) - \Delta T_{h,i}(k)) & \Omega_{h,i}(k) > 0 \end{cases} \tag{4.2.4}$$

Aside from flow and temperature measurement accuracy concerns at the VAV box, there are several limitations to the above approach for estimating reheat power. The conditions in the building (e.g., temperature in the return plenum, supply air flow and temperature, etc.) are dynamic, so the temperature differential measured when the coil was last closed for an extended period may not be representative of the temperature difference when the coil is open, especially if the coil has been open for an extended period. Additionally, this approach ignores distribution losses (the heat lost from piping when a valve opens and closes), and the heat lost from the coil once the valve closes. Lastly, when the zone temperature is just above the zone heating setpoint, the reheat valve will be closed and thus, the reheat power estimate will be zero for that zone. Clearly, moving to a candidate SAT that is lower than the current SAT will cause this valve to open, and the coil will consume reheat energy. This estimation method above does not capture this secondary effect directly. However, it will capture this effect in the subsequent iteration of the SAT reset control - once the SAT moves to the new candidate setpoint, and the reheat valve opens.

Similarly, the following equations describe the cooling power calculation:

$$\Delta T_c(k+1) = \begin{cases} \alpha\left(T_s(k+1) - T_m(k+1)\right) + (1-\alpha)\Delta T_c(k) & \Omega_c(k) = 0 \\ \Delta T_c(k) & \Omega_c(k) > 0 \end{cases} \tag{4.2.5}$$

$$P_c(k+1) = \begin{cases} 0 & \Omega_c(k) = 0 \\ \sum_{i=1}^{n} \rho c_p \max(0, \hat{V}_i(k)(T_m(k) - T_s^{sp}(k+1)) + \Delta T_c(k)) & \Omega_c(k) > 0 \end{cases} \tag{4.2.6}$$

Cost estimation and new setpoint calculation

Using time-of-use prices for electricity, cooling and heating, we can map the estimated reheat, chilled water, and fan power values to cost estimates. We sum these individual cost estimates to yield a total cost estimate at each candidate SAT setpoint, and then select the lowest total cost candidate as the new SAT setpoint.

$$\min_{T_s^{sp}(k+1)\in\mathcal{M}=\{T_{s,1}^{sp},\cdots,T_{s,p}^{sp}\}} \hat{C}(k+1) = c_{elec}\left(P_f(k+1) + P_c(k+1)/COP\right) + c_{hw}P_h(k+1) \tag{4.2.7}$$

4.3 Summary

In this chapter, the cost-responsive control strategy is proposed with minor modification from current rule-based control. The existing best practice is model-free and easy to debug and interpret the control law. The cost-responsive control strategy for the supply air temperature setpoint incorporates the energy model to achieve the minimum energy cost in one-step ahead. The saving performance highly depends on energy and cost model accuracy, but it can provide building-specific improvement.

Chapter 5

Case Study: Experiments

Apart from simulation-based studies, experimental verification is necessary to build confidence for widespread implementation.

5.1 Case study building

We implemented the control strategies in Sutardja Dai Hall (SDH), an institutional building of 13 000 m^2 on UC Berkeley campus. It is divided into a four-floor nanofabrication laboratory and a seven-floor building containing open-space and private offices, and also houses a few classrooms, research labs, an auditorium, and a café. This seven-floor building is used as the testbed for model identification and control algorithm verification. The building is equipped with Siemens Apogee BMS and sMap package through BACnet network protocol interface [46], which yield the convenience and ease of access of the control system and data. The HVAC system has one centrifugal chiller and one absorption chiller, which operate in parallel with only one running at a time. There are total 138 thermal zones, of which the majority (121 zones) have hot water heating coils. We restrained the experiment and analysis to occupied hours, i.e. 6am-8pm, in order to ensure the results are comparable to more typical office building operations.

The default, manufacturer-provided controller used PID loops to actuate the VAV boxes with single-max control logic and uses trim-and-response to reset the supply air temperature. The time-series data with meta information is collected every 1 minute and archived on OpenBMS [53]. We choose a period of 15 minutes to resample the data for the purpose of modeling.

5.2 Power cost estimates

Aside from the hot water, chilled water, and fan power estimates, we also need a common basis for directly comparing them. We chose dollars per hour, as this seemed like the most relevant, however, it would also be valid to use site or source energy, or other similar metric.

We used the UC Berkeley campus estimate of $0.023/kWh for steam as the hot water cost estimate, as the campus district steam cogeneration system converts to a hot water system inside SDH. This underestimates the cost of hot water as the conversion process also includes losses which we were unable to easily quantify. This approach also ignores pumping power costs. It is also worth considering that a district steam cogeneration system is also relatively unusual. In comparison, a typical gas fired hot water boiler system would approximately double the cost per unit energy of hot water.

We used a fixed system coefficient of performance of 5.0 to convert the chilled water power to an electrical power value. This inherently assumes that chilled water consumption instantly corresponds to electrical power consumption, which is not the case in reality, and causes minor errors when the cost of electricity changes during the day. Also, the simple fixed COP estimate approach could be improved with a chiller model of varying degrees of complexity, but we deemed that to be outside the scope of this project.

For electricity consumption, we used the actual tariff data from the utility provider for this building which varies from $0.074/kWh in winter off-peak to $0.097/kWh in summer peak cost category periods. Note that we do not include the daily per meter charges, or power factor correction charges, transformer losses, and transmission losses, each of which are a relatively minor part of the overall electricity cost. However, we also do not include the demand charges which are based on the monthly peak demand value within each cost category period, as that would require knowledge of the total campus electricity demand - information that was not readily available. It would also require a prediction of what exact time of the month the peak demand was expected to occur within each cost category period, and then applying an exceptionally high $/kWh cost during that window of time so that the optimal SAT would effectively prioritize minimizing electricity use over everything else (ignoring hot water use entirely). This would significantly complicate the proposed solution, and is a significant negative implication of these types of pricing structures on energy conservation measures in practice. These demand charges are significant - ranging from $8.31/kW in the winter off-peak to $24.06/kW during the summer peak period - and are approximately equivalent to 30-50% of the overall cost of electricity depending on when they occur, and how much electricity the AHU is consuming

at that time. Incorporating these peak demand electricity costs would reduce the relative cost of hot water power and reduce its effect on the optimal SAT. In this particular building, that effect is already very minor.

5.3 Randomized controlled trial

Thoroughly testing the effectiveness of an intervention in a building is a challenge due to the varying nature of weather, building occupancy, usage, HVAC setpoints, etc. For most Measurement & Verification activities, 12 months of pre (i.e., "baseline") and post (i.e., "intervention") data is the recommended amount of data, though recent research has shown that the results from 6 months of data yield similar results in most cases [54]. The concern always arises that something substantial may have changed in the building which is unrelated to the intervention that the analyst wishes to evaluate, and then confounds the results. For many interventions in buildings, it is only possible to test pre- and post- intervention and there is simply no choice in the matter. For example, physically replacing a chiller or boiler. However, for interventions that consist purely of changes to the control strategy in a building, it is feasible to perform a randomized controlled trial i.e., randomly switch back and forth between the intervention and the baseline control sequences. This approach is far more robust as any changes in building operation will simply cancel each other out by the random selection process given a sufficient sample size.

We ran an experiment in SDH for 6 months, from September 1, 2016 to February 21, 2016. During this time, we randomly selected between two different supply air temperature reset strategies every day at midnight. In the following, describes the industry best practice trim and respond logic with constraints based on outside air temperature as the Baseline throughout, and describes the proposed new reset strategy as the Intervention throughout. After discarding unrepresentative days in which this experiment was not running due to other experiments being performed in the building, or when scheduled maintenance or communication issues occurred, the random selection yielded 77 days of "Baseline" data and 68 days of "Intervention" data, collected at 5-minute intervals.

5.4 Results

The total HVAC energy cost was \$0.43 /h (or 17%) lower during the intervention period than the baseline period. Figure 5.1 compares the total HVAC cost of the two control strategies and shows that the intervention generates significant cost savings.

These savings occur under different operating conditions, during which times the building loads and outside air temperature distributions are quite different.

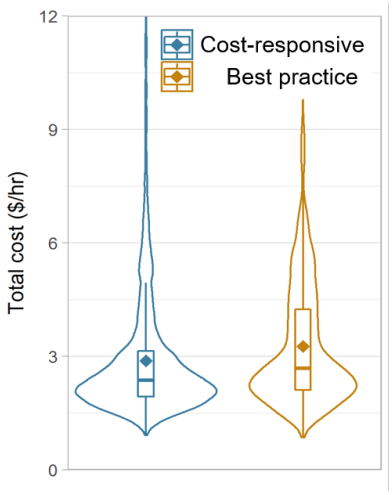

Figure 5.1: Total HVAC cost for the two control strategies.

Figure 5.2 shows that there are large differences between the supply air temperatures selected by the two control strategies at the same outside air temperatures. The intervention strategy uses notably higher supply air temperatures when it is warmer, and lower supply air temperatures when it is moderate. The SATs converge to the same value the upper limit of the SAT range - at lower outside air temperatures. However, at higher outside air temperatures they are almost exactly opposite. This is particularly the case during periods when there is little load, such as during weekend. The intervention strategy tends to maximize the use of outside air economizer, indicated by the proximity of the SAT to the black line (where SAT and OAT are the same). It is important to note that the cost-optimal control shown in Figure 5.2 is unique to this building, its HVAC system, the electricity and steam cost, and how it is currently occupied and operated. Though the outside air temperature is the dominant factor (at least in this case), a regression against outside air temperature alone cannot identify the optimal SAT. The optimal SAT for a given condition varies widely depending on a range of parameters.

There is also far more scatter in the supply air temperature data for the intervention strategy than for the baseline. This is particularly the case during the weekday, when loads are more variable and there is likely to be more comfort driven cooling

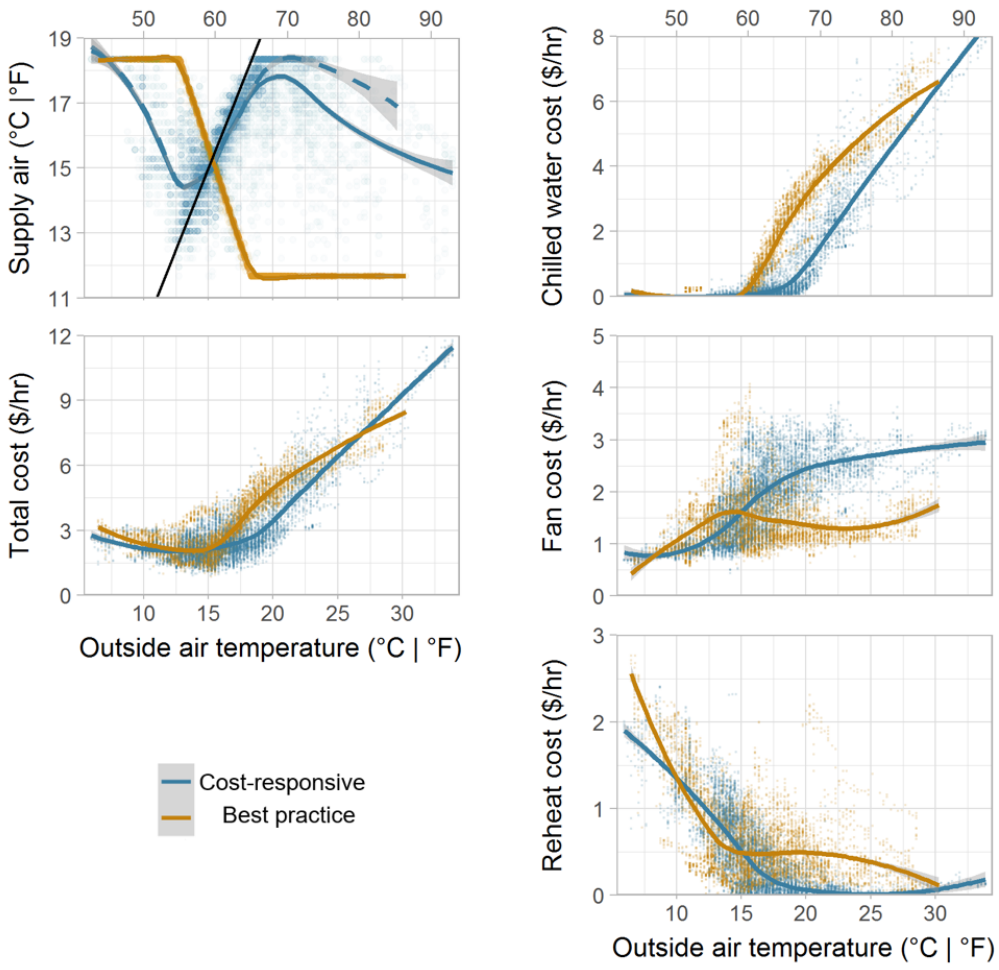

Figure 5.2: Scatter plot of the total energy cost and supply air temperature by the outside air temperature.

requests. This indicates that the new control strategy is responding dynamically to the conditions in the building at that time, and finding the point of lowest cost.

Figure 5.2 also shows that total HVAC energy cost closely correlates with the outside air temperature, as one would expect. It clearly shows that the intervention strategy matches or outperforms the baseline strategy under all conditions. The savings generated by the intervention also depend highly on outside air temperature, and are largest in the range from approximately 15.6 C (60 F) to 23.9 C (75 F). For context, in this climate, the outside air temperature is within this range for just over

half (53%) of typical office occupied hours (8am to 6pm) throughout the year.

The breakdown of cooling, fan, and reheat costs illustrates that in general, the intervention strategy trades an increase in fan energy cost for a larger reduction in cooling and reheat energy costs combined. Quantifying this by directly comparing the intervention and baseline datasets over the entire study period shows that fan energy cost increased by \$0.24/hr (19%), while chilled water energy cost decreased by \$0.57/hr (63%) and reheat decreased by \$0.09/hr (24%), yielding the overall decrease in total HVAC energy cost of \$0.43/hr (17%) noted above.

Similarly, Figure 5.3 shows similar trends against the time of day, which is presumably a proxy for load within the building (as well as outside air temperature).

5.5 Limitations

The three individual cost functions are convex and monotonic 5.4 within the evaluated range of feasible SATs within the 5-minute iteration time interval. This ensures that there is only one global minimum cost for the SAT to converge towards, and this assumption applies reasonably well to the heating and fan power estimates. It also applies to the cooling power estimates when a central chilled water plant supplies the cooling. However, for packaged DX AHUs, there is a significant energy cost penalty to using a small amount of cooling - the energy cost function is not continuous at this point. This will pose issues in implementation, or will yield less than optimal results if ignored. For example, for many of the operating hours in the SDH study, the cost-responsive reset converged to an SAT setpoint that was just above or below the point where cooling was needed. If this was a packaged DX unit, it would ensure that the compressors cycled frequently, which is far from ideal. Thus, this control strategy is widely applicable to buildings with VAV systems served by chilled water plans and reheat served by hot water plants. The control strategy can likely be extended to DX cooling and electric heat with additional research.

The other limitation to application is in climates with significant dehumidification loads, as mentioned previously. While this is not a major issue in dry climates (e.g. many climate zones in California), it would be for other climates. Given the lack of robust and reliable sensors for measuring moisture content in air (e.g., humidity, enthalpy, or dew-point sensors), and the fact that these are not common within most AHUs, this is a significant limitation in climates where latent cooling makes up a significant portion of total cooling. However, the control strategy can likely be extended to account for dehumidification costs with additional research, and/or could be modified to function with an additional constraint for dehumidification control. For example, we could use the typical meteorological data for each location

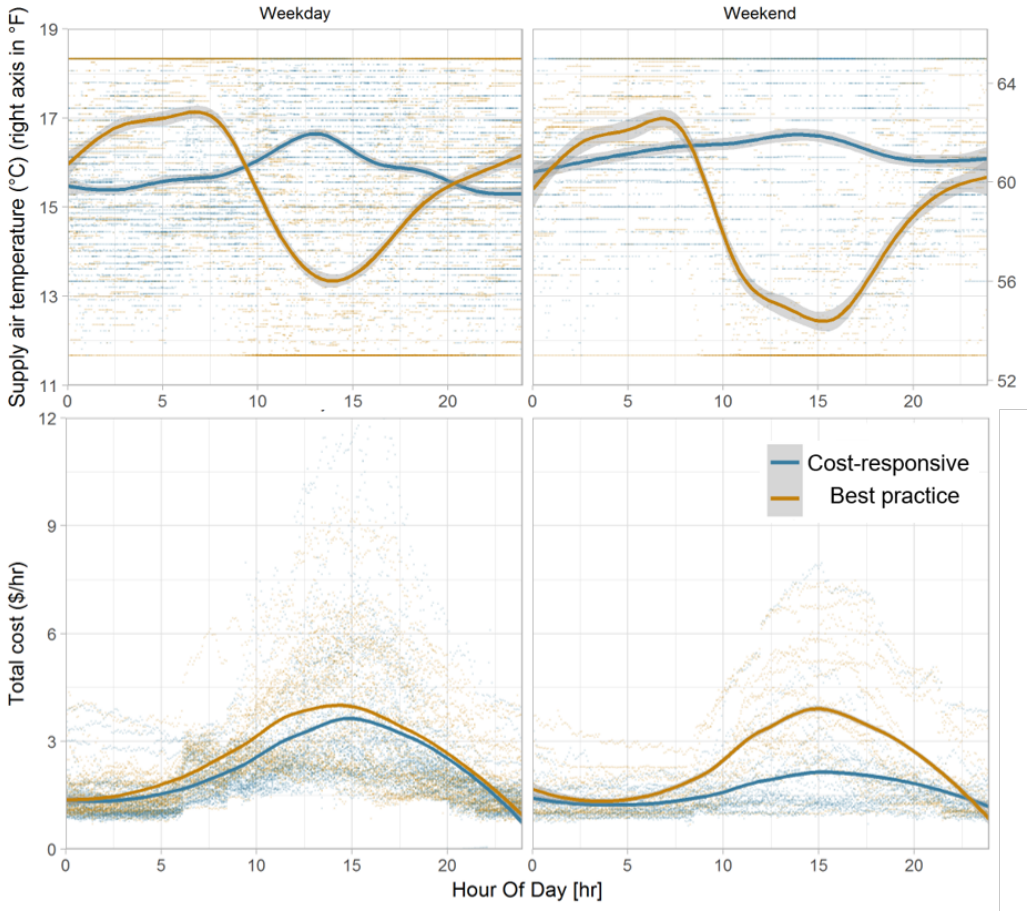

Figure 5.3: Scatter plot of the total energy cost and supply air temperature by the time of day.

to calculate a coefficient that increases the cooling cost calculation (see Equation 6) to account for typical dehumidification at a particular combination of SAT and outside air temperature. This is an approximate approach, but it simply uses weather data (information that is readily available at no cost), and does not require additional instrumentation.

Note also that though all SAT reset strategies will affect indoor humidity levels, neither the proposed cost-responsive SAT reset, nor the existing best practice SAT reset, address humidity control as this is not common in air handling units outside of applications in clean rooms, hospitals, museums, and other demanding environ-

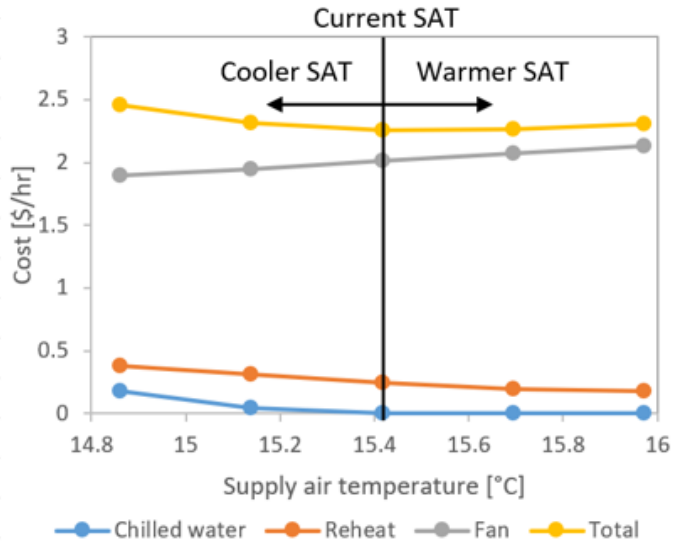

Figure 5.4: Example of cost estimation for a small range of SAT setpoints around the current setpoint.

ments. Instead, in most applications humidity is controlled implicitly by the upper limit placed on feasible SAT setpoint values. In other conditions, or where those humidity levels are of concern, either the upper SAT setpoint limit should be lowered accordingly, or the AHU control logic should include sequences to explicitly address humidity control.

We expect the energy savings results to vary quite widely between buildings, and that this will depend on a wide variety of factors. While SDH is a reasonable representation of many buildings in regard to the first three points, the same does not apply for the last three. SDH has a slightly wider zone setpoint temperature range than usual due to the use of Comfy, and the building operates continuously. Neither of these are representative of a typical office building and thus, extrapolating the magnitude of the energy savings results of this study to other buildings is not valid. SDH also uses the relatively unusual combination of single-max controls (i.e. relatively high zone minimum airflow setpoints), and demand based supply air temperature resets. Lastly, the mild climate has more operating hours within the range of outside temperatures that provide larger energy savings than many other climates. Further implementations in other buildings and simulation-based analysis are valid methods to estimate the energy savings potential in a broad population of

buildings.

5.6 Summary

In this chapter, the cost-responsive supply air temperature setpoint reset strategy is implemented in a office building. Compared the energy costs to the industry best practice in a randomized controlled trial, it shows approximately 17% energy cost reduction. Though there are some limitations that require further research, the proposed control strategy is applicable as it can be implemented within many existing building management system.

Chapter 6

Case Study: Monitoring-based Commissioning

As time goes by, the operational efficiency of the building will decrease due to multiple reasons: operators override systems, mechanical systems degrade, and management system turnover. Commissioning identifies and implements operational and maintenance measures in building to make it perform as expected. An existing classroom building is used as a case study to demonstrate the process of commissioning.

6.1 Case study building

Located in the east side of the Berkeley campus, the Haas Complex, constructed in 1995, consists of three connected buildings, i.e. the Faculty Wing, the Student Services Wing and the Cheit Hall. The three buildings are connected through two sky bridges. Cheit Hall, a four-story classroom building with a total floor area of 27;000 m2, is one of the three buildings in the complex that serves about 2,000 students the Haas School of Business1. Classrooms are on Floor 1-3 in Cheit Hall. The AHUs, the chillers, as well as many other machines are located in the machine room on the fourth floor.

The BMS used by Cheit Hall is from AutomatedLogic, which provides a WebCtrl interface to view and download various kinds of data about the HVAC system.

6.2 Occupant Survey Analysis

A recent survey on the IEQ in the Haas Complex was conducted to the staff and faculty occupants in the Faculty Wing and the Student Services Wing. The valid

response rate of the 100 questionnaires is 97%. Overall, there are some aspects to improve, such as the thermal comfort and the cleaning service.

Thermal Comfort

In the responses, most respondents reported that the ventilation is poor and the air is stuffy. Besides, the thermostats are either not accessible or not working. During hot weather, the indoor temperature can be even higher than the outside, and the fans are of little help. The building has distinct micro climates, especially during summer. South-facing offices are hotter than north-facing ones.

Ventilation

Another issue is ventilation. Due to the limited space in a shared room, ventilation is necessary to maintain the air quality and comfortable temperature. There are two kinds of ventilation: natural ventilation through windows, and mechanical ventilation via AHUs. When it is noisy outside or no windows can be opened, the mechanical ventilation system is essential for ensuring the IEQ. Lack of ventilation is also one reason accounting for the mold appeared on the walls and the ceiling tiles.

Many occupants complained that the air is stuffy and the temperature inside is even hotter than outside during summer. Trash and wasted food even make the situation worse. If there is enough ventilation, the air will not smell so bad. It needs to be further investigated why the air circulation is not effective and efficient.

After all, there seems to be a correlation between thermal comfort and ventilation. When people feel hot, they also tend to feel stuffy as well.

6.3 Energy Benchmarking

For benchmarking the energy use of the Haas Complex, we chose the period between August 2014 to July 2015. Using the parameters shown in Table 6.1, we get the EnergyStar benchmarking result, including the source and site EUI, as shown in Table 6.2.

It is interesting to see that the Weather Normalized site/source EUI is exactly the same as the site/source EUI. It probably implies that the energy consumption of the property does not exhibit a correlation with the temperature. One possible explanation is that the ventilation systems run all year around, regardless of temperature. Also, the temperature in Berkeley does not fluctuate so much during our evaluation period. Therefore, the energy use during 30-year average weather conditions will be

the same as current year result. Another interesting finding is that site/source EUI is not exactly the result of site/source energy use divided by the gross floor area.

Occupancy	Gross Floor Area	Weekly Operating Hours	Enrollment	Number of FTE Workers	Number of Computers
100%	200,000 ft^2	92	2,000	350	1,000

Table 6.1: Parameters used in the EnergyStar benchmark system.

Metric	ENERGY STAR score	Source EUI (kBtu/ft^2)	Site EUI (kBtu/ft^2)	Source Energy Use (kBtu)	Site Energy Use (kBtu)	Total GHG Emissions (Metric Tons CO_2)
Current	Not Available	368.0	206.9	73,601,979.8	41,386,793.0	2,934.1
Median Property	50	262.6	147.7	52,517,999.5	29,531,154.7	2,093.6

Table 6.2: EnergyStar benchmarking result.

The total energy consumption in the Haas Complex shows a general decreasing trend, as shown in the upper graph in Figure 6.1. The quarterly energy consumption is highest during Q2 and Q3, during the "hot season". The energy consumption is decreasing monotonically over the years for Q3 and Q4, but the trend is sporadic for Q1 and Q2. Q3 and Q4 cover the hotter seasons, and the current trend implies the cooling energy consumption is becoming more efficient over years, but the heating mechanism has not improved. Therefore, in the project we have dedicated a significant amount of effort on studying, and improving the heating mechanism in Haas Cheit Hall.

6.4 Ventilation

According to the ANSI/ASHRAE Standard 62.1-2013[16], the minimum ventilation rate for classroom is the combination of outdoor air 7.5 cfm/person and 0.06 cfm/ft^2, while the default values for combined outdoor air is 0.15 cfm/ft^2. Meanwhile, Title 24 [18] suggests 15 cfm/person. It is recommended that the indoor CO_2 concentration should be kept under 1000 ppm to maintain enough ventilation. Figure 6.2 is a heat map showing the typical CO_2 variation within a day in the selected classrooms in Cheit Hall.

The CO_2 concentration exceeds 1000 ppm several times a day, even when the local air flow rate reached its maximum. At the same time, the economizer damper is closed, so the proportion of the outside air in the mixed air is minimum, and hence the CO_2 concentration couldn't be decreased. As a result, the discharged air with high CO_2 concentration is circulated into the classrooms again.

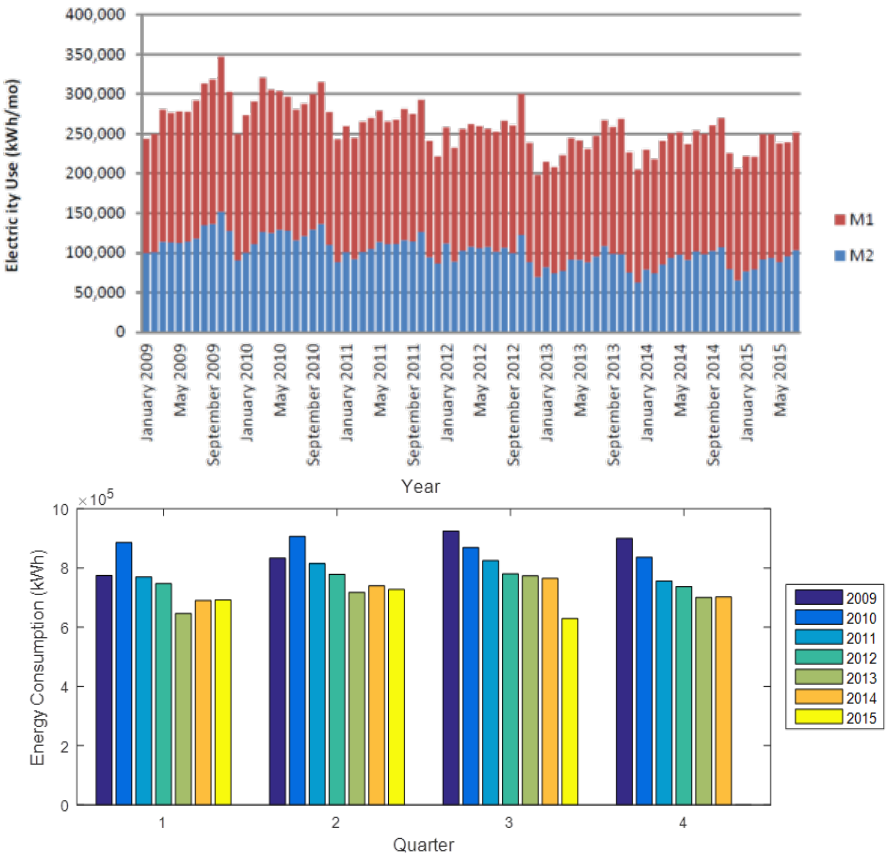

Figure 6.1: Haas complex annual energy consumption 2009-2015.

Figure 6.3 shows the situation of C135 on Nov 12 2015 in a more detailed way. As can be seen, the CO_2 concentration is sensitive to both the occupancy and the airflow rate. While Figure 6.4 shows the economizer damper position on the same day. The CO_2 concentration of outside air is about 450 ppm and when the economizer damper opens to its maximum, the CO_2 concentration of room C135 cannot increase so dramatically, as shown during 13:00-14:00 time period.

6.5 Heating Profile Analysis

The reheat system can provide relatively precise control of space temperature, but can be very energy intensive. Analyzing the heating pattern can reveal insightful

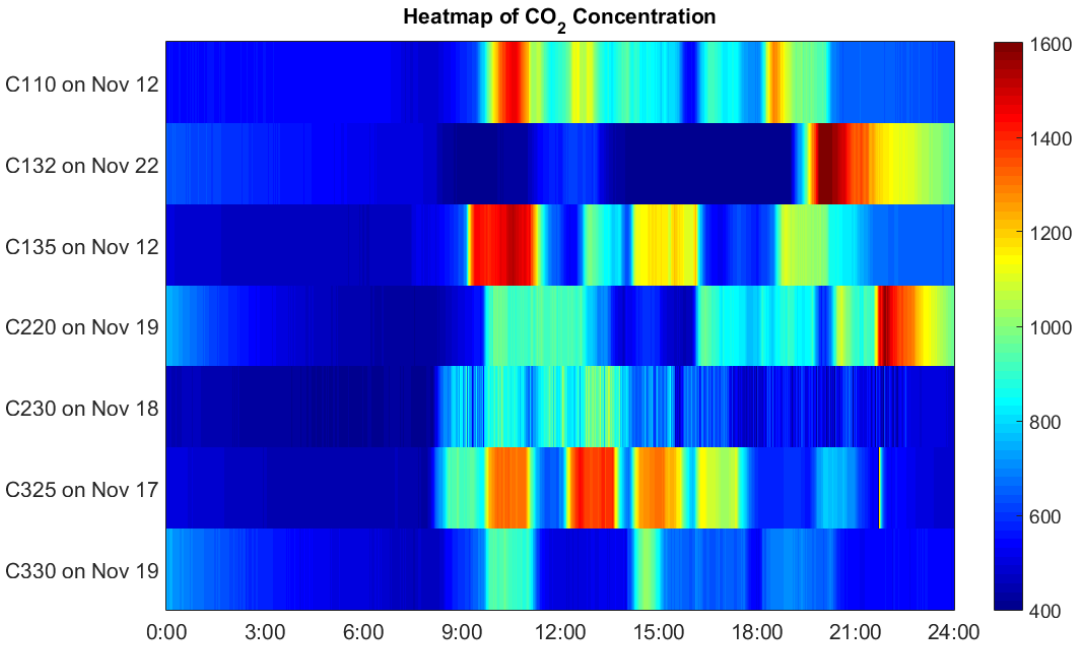

Figure 6.2: A heat map showing the typical CO_2 variation in seven classrooms in Cheit Hall.

potential for energy savings. In this section, we use statistical learning method to uncover the underlying existing issues in the system.

To qualify and quantify the amount of reheat, there are two variables that are relevant, the temperature difference between discharge air temperature to each room and supply air temperature leaving the AHU, and the hot water valve position for each VAV/CAV box.

Hot water valve position profile

Data The data used in this section contains the daily hot water valve opening position (HW%) for 30 rooms at 5 minutes intervals. We only consider the data during occupied hours in weekdays, i.e. Monday-Friday 6:30AM-9:30PM. Figure 6.5 shows the heatmap of data for 30 rooms at 13 days. Each pixel on the graph represents the opening of the hot water valve at a certain time instance on a particular day, while the color of a pixel represents the degree of opening as indicated as the

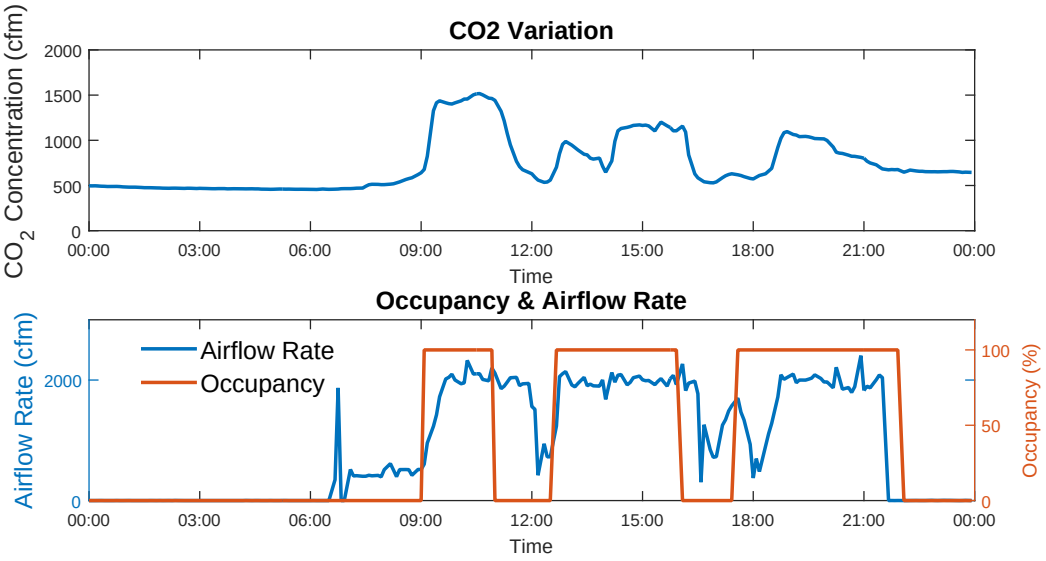

Figure 6.3: The CO_2 concentration, with respect to its occupancy and air flow rate. The occupancy data is obtained from the class schedule, assuming the classroom is 100% occupied during class period and unoccupied at other times.

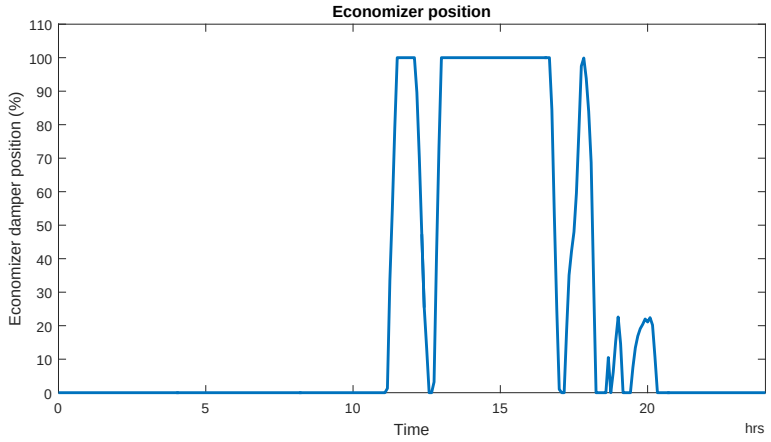

Figure 6.4: The economizer damper position on Nov 12 2015.

color bar. The histogram on the left represents the total HW% for a particular VAV/CAV box on one day.

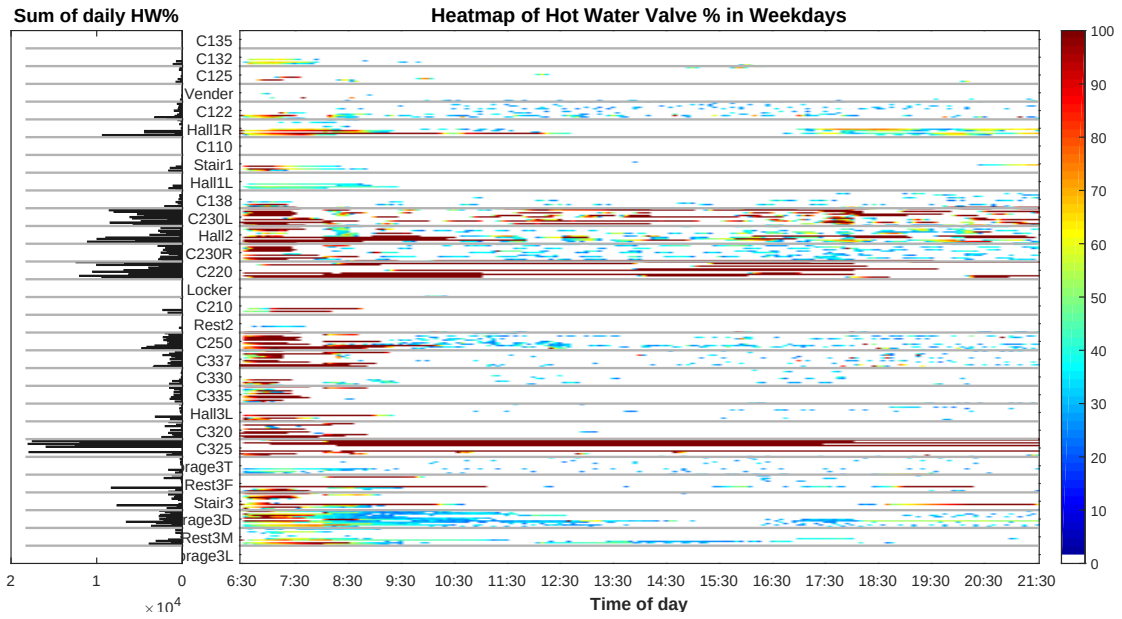

Figure 6.5: The hot water valve position profile for all rooms in weekdays.

We simply decompose the daily HW% profile $l(t)$ as $l(t) = as(t)$, where $a = \sum l(t)$ and $s(t) = l(t)/a$. a is the daily total usage and $s(t)$ is the normalized usage profile, which denominated as *usage shape*.

Daily total usage a characterization The simplest characterization of daily total usage a is to infer probability distribution of values across the population. The empirical distribution exhibits a long right tail and the range of a is quite large with limited sample size. Since the sample size is not so large, parametric distribution fitting method, such as mixture Gaussian distribution, cannot be adapted properly. Therefore, a Kernel distribution (Eqn. 6.5.1) is utilized to model the distribution of $log(1 + a)$ instead of a. The result is shown in Fig. 6.6. The distribution model can be used to predict the future daily total usage for each room.

$$\begin{aligned} \hat{f}(x) &= \frac{1}{nh} \sum_{n}^{n} K(\frac{x - log(1 + a_i)}{h}) \\ K(t) &= \frac{1}{\sqrt{2\pi}} exp\left(\frac{-t^2}{2}\right) \end{aligned} \tag{6.5.1}$$

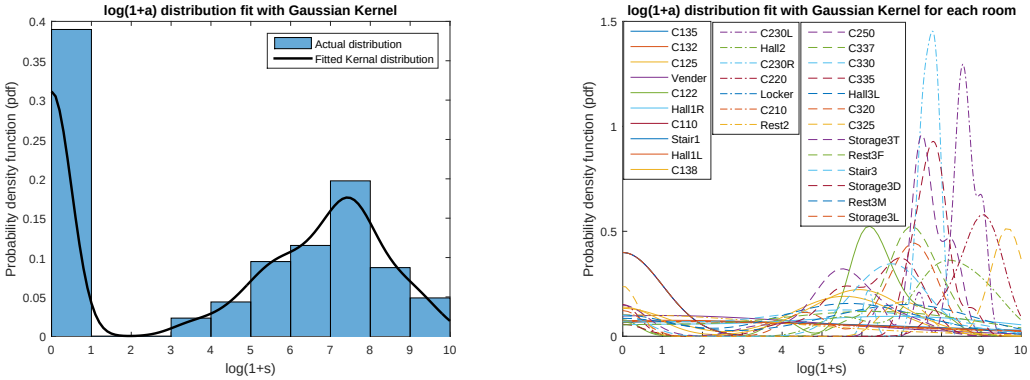

(a) Air Handling Unit (AHU)

(b) VAV/CAV box

Figure 6.6: The Gaussian Kernel distribution fitting on $\log(1+a)$ for all and for each room.

The maximum likelihood estimate of $log(1+a)$ and corresponding probability density for each room is listed as Tab. 6.3.

From the result, we can find that four rooms, C135, C110, Locker,and Storage3L, do not use hot water valve at all, i.e. $a = 0$; some rooms seldom use reheat, Rest2, C132, Vender, C210 and Hall1L, i.e. a is small; while some rooms use reheat intensively, C325, C220,C230L, Hall2, Store3D and C230R, i.e. a is large. Combined with the probability density value, we can easily divide the room into four categories.

- *use heating rarely* 10 rooms
  C135, C110, Locker, Storage3L, Rest2, C132, Vender,Hall1L, C125
- *use heating constantly and intensively* 4 rooms
  C325, C220, C230L, Hall2
- *use heating constantly but not intensively* 6 rooms
  Storage3D, C230R, C250, C337, C335, C320
- *use heating varying a lot* 10 rooms
  C122, Hall1R, Stair1, C138, C210, C330, Stair3, Storage3T, Hall3L, Rest3F, Rest3M

HW% usage shape $s(t)$ clustering At first step, we eliminates the profiles with $a = 0$.

Room	C135	C132	C125	Vender	C122	Hall1R	C110	Stair1	Hall1L	C138
MLE	0	0.9485	5.5600	0.9964	6.2002	6.8824	0	1.7202	1.3591	5.9670
Density	0.3988	0.0760	0.1904	0.0989	0.5245	0.0950	0.3988	0.0760	0.1904	0.0989
Room	C230L	Hall2	C230R	C220	Locker	C210	Rest2	C250	C337	C330
MLE	8.5335	8.2254	7.7640	9.0793	0	0.6763	0.2273	7.5079	7.2877	5.6012
Density	1.2965	0.3621	1.4537	0.5792	0.3988	0.0707	0.1019	0.9615	0.5231	0.1254
Room	C335	Hall3L	C320	C325	Store3T	Rest3F	Stair3	Store3D	Rest3M	Store3L
MLE	7.0077	5.6565	7.3284	9.6061	5.5383	6.2614	6.7074	7.8028	7.1173	0
Density	0.3731	0.1563	0.4438	0.5117	0.3213	0.1186	0.3454	0.9282	0.1511	0.3988

Table 6.3: The MLE of $log(1+a)$ and corresponding density for each room.

First, we apply the simple K-Means algorithm with a fixed clustering size k. This method can only guarantee an optimal distance between cluster centroids, but not limit the distance between each sample and its corresponding cluster centroid. Because the usage shape sample size is not big enough and the difference among the population is quite huge, a lot of samples will be clustered in one class while other clusters only contain single spike shape, as shown in Fig. 6.7.

To ensure every usage shape is within a certain range of the cluster centroid, we can use a two-stage clustering method[55]: first use adaptive K-mean algorithm with a specific threshold, then merge clusters whose centroids are too close. The result is shown in Fig. 6.8. It gives almost the same result as simple K-means. The ones with few spike would be clustered as single class.

Since the data size is small, we can classify the data based on selected feature. Many possible features can be extracted from usage shape $s(t)$, such as peak usage fraction, peak time and peak duration. The Fig. 6.9 show some representative shapes.

• *Number of peaks*
If we take a look at the number of peaks of $s(t)$, it is worth noting that there are certain amount of usage shape that exist more than 20 peaks, as shown in Fig. 6.10, which means that the hot water valve need to open and close a lot. The oscillation effect can result in energy inefficient and inaccurate temperature control. If we apply

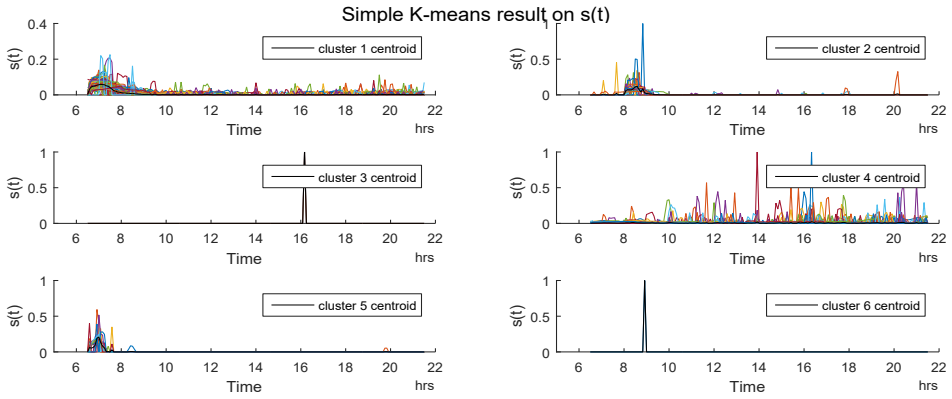

Figure 6.7: The example of simple K-means result with $k = 6$.

the two-stages K-means to data with specific peak number, then the result will be a lot of better than previous, as shown in Fig. 6.11.

- *Morning peaks (6:30-8:00am)*

From Fig. 6.5, the morning peaks happen a lot. It is worth to classify the usage pattern according to peaks in morning. There are three rooms whose heating usage happening in morning takes up to 80% of total daily usage: C335, C320 and Stair3.

Effectiveness of hot water valve

In this part, we analyze the relationship between DAT-SAT and HW% to determine the effectiveness of hot water valve. The pairs of data are shown in Fig. 6.12 for each room. And we cluster the data into three categories as shown in Fig. 6.13a.

If we summarized the clustering result into Fig. 6.13b, the effectiveness of hot water valve can be divided into three types.

- *faulty (do not heat up)* 3 rooms
  C230L, C220, C325
- *never use valve* 4 rooms
  C135, C110, Locker, Storage3L
- *effective reheat* 13 rooms
  other rooms

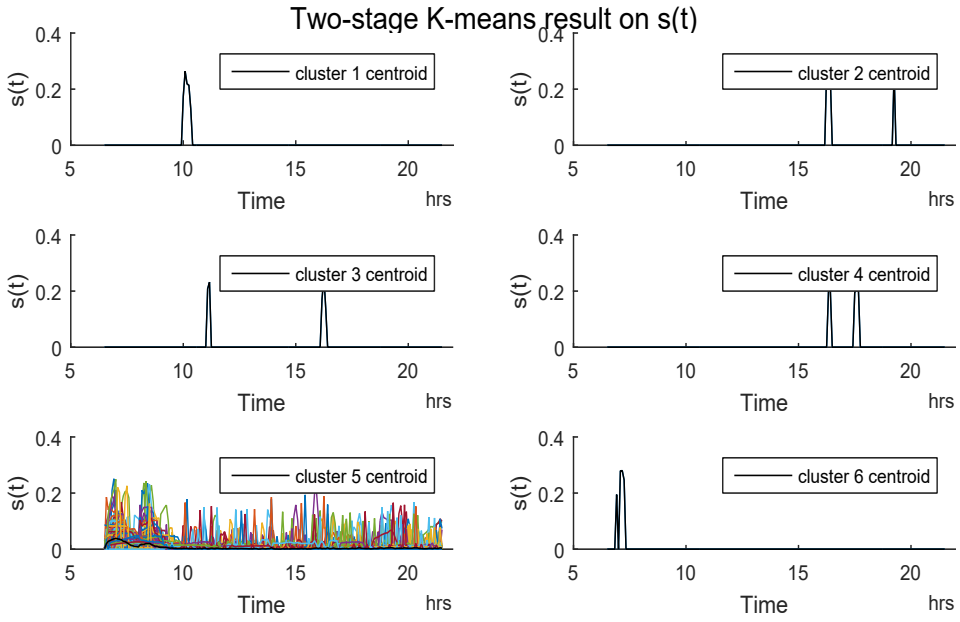

Figure 6.8: The example of two-stage K-means result with $kmin = 6, \rho = 0.5$.

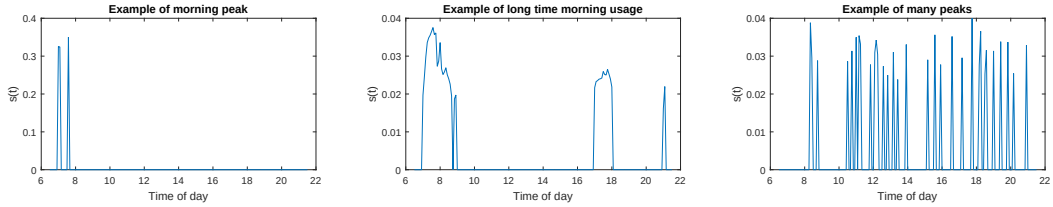

Figure 6.9: Some examples of representative shapes.

Recall the result in Section 6.5, the three faulty VAV boxes are categorized in *constantly and intensively heating*. Because the heating coil cannot really heat up the air, the controller will keep request opening the hot water valve, which resulting in the huge amount of a.

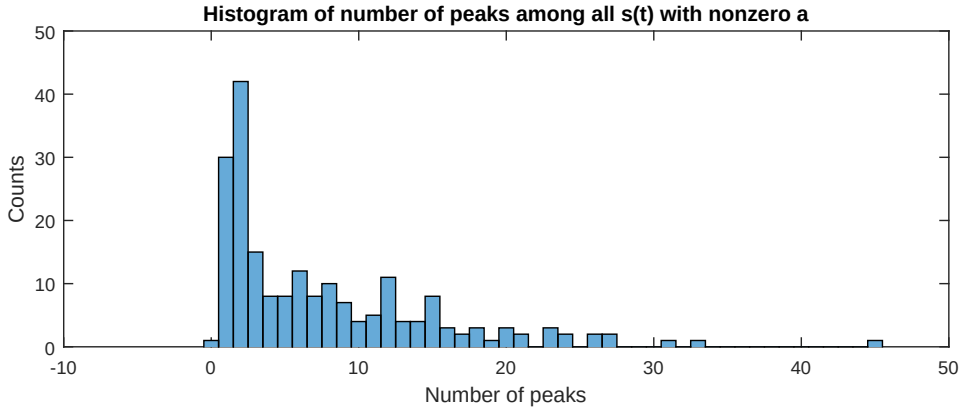

Figure 6.10: The histogram of number of peaks in one usage shape.

6.6 Summary

This chapter is about how to use the operational data to identify the reheat and ventilation issues in Haas Cheit Hall. The findings are classified into two categories: thermal comfort, and ventilation. On the thermal comfort side, excessive reheat exists, which implies the supply air temperature was often overly low. Three malfunctioning hot water valves were identified, which not only caused excessive energy consumption, but also supplied unnecessary extra cool air to the local classrooms. On the ventilation side, five classrooms were identified to be under-ventilated according to the CO_2 amount measured during the occupied hours.

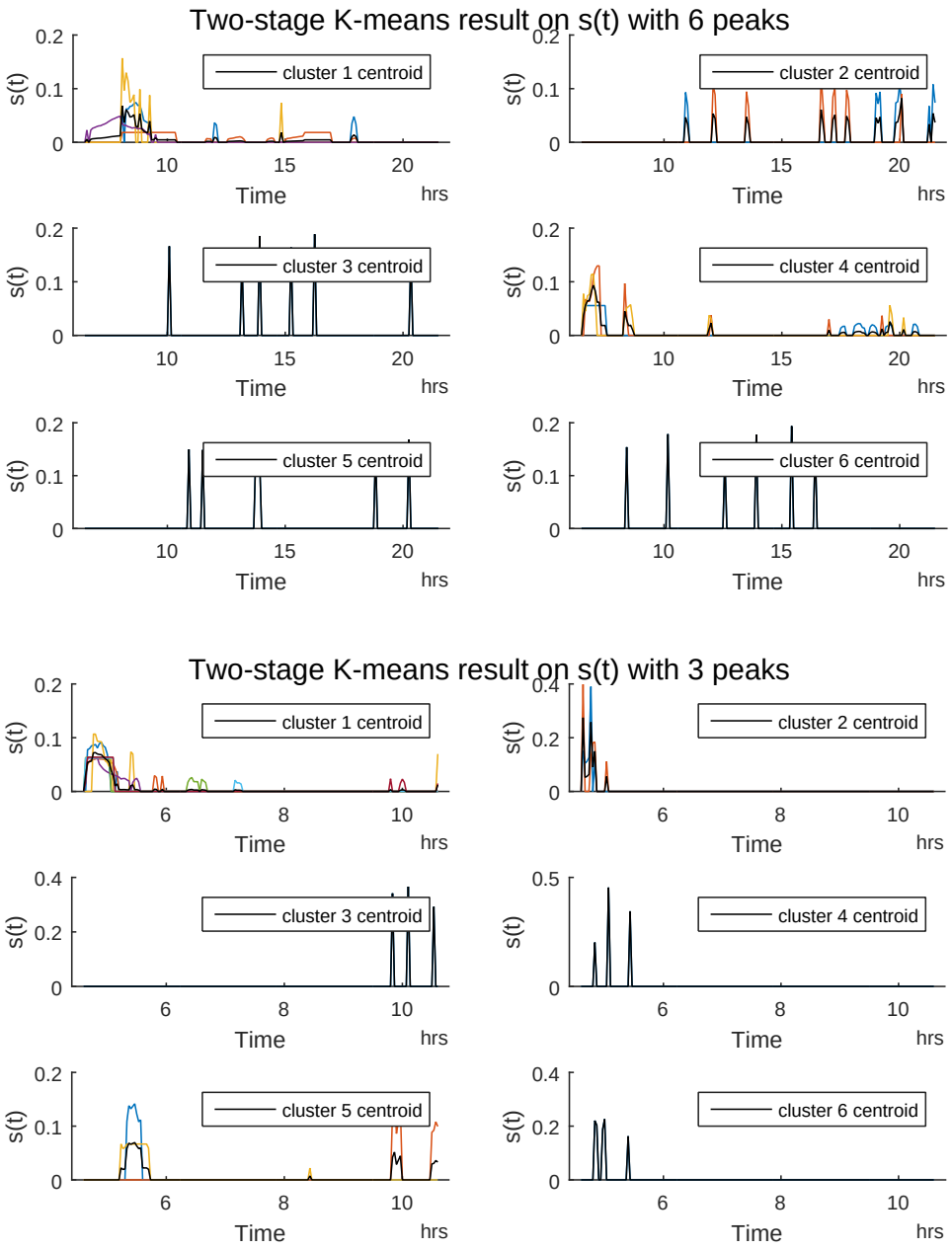

Figure 6.11: Examples of two-stage K-means clustering on data with certain peak number.

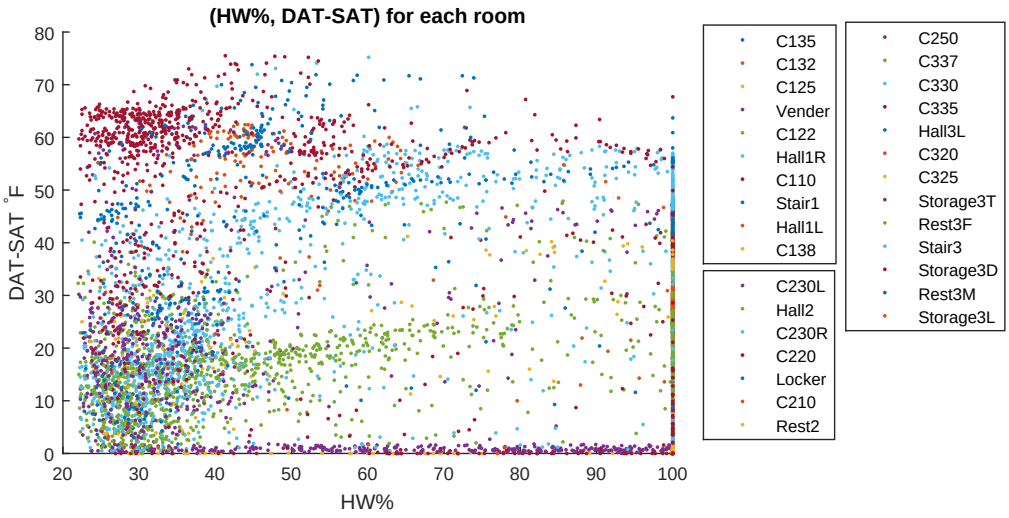

Figure 6.12: The pairs of hot water valve and temperature difference of SAT-DAT.

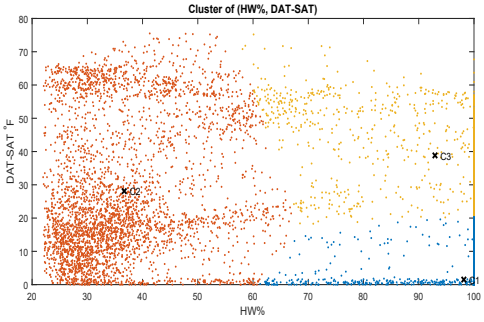

(a) The clustering result of Fig. 6.12.

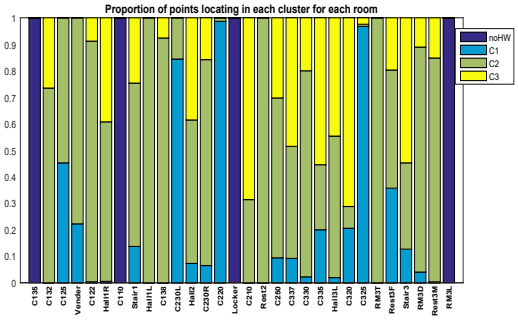

(b) The summary of cluster result for each room.

Figure 6.13: Clustering result of hot water valves

Chapter 7

Case Study: Retrofitting to Net Zero Energy Building

The design of retrofitted energy-efficient buildings is a promising option towards achieving a cost-effective improvement of the overall building energy performance. An existing office building is used as a case study to demonstrate the process of retrofitting planning using simulation.

The office building, as in Figure 7.1 is located in Los Angeles, California. It was previously a warehouse built in 1939 and then has been renovated and converted into office space in 1972. The building has around 400 square meters of existing photovoltaic arrays, which offers an opportunity to utilize preexisting solar panels to achieve zero net energy use.

7.1 Climate analysis

The climate is a hybrid of two Southern California micro-climates. It is far enough inland that one can feel the immense heat radiated by numerous miles of asphalt and the densely built environment, yet close enough to the coast that remnants of California's coastal sea breeze percolate through the nearby hills cooling the neighborhood considerably. At the peak of summer, daily temperatures often reach the high eighties and seldom reach a sweltering ninety degrees. Although ninety may be very warm, the real discomfort comes when the breezes seize. In winter, daytime temperatures remain in the low seventies. As with summer, the temperature of the air is usually pleasant, while the breezes may bring a slight chill.

As seen in the climate trend 7.2 using Typical Meteorological Year Data(TMY), that climate is rather stable and consistent.

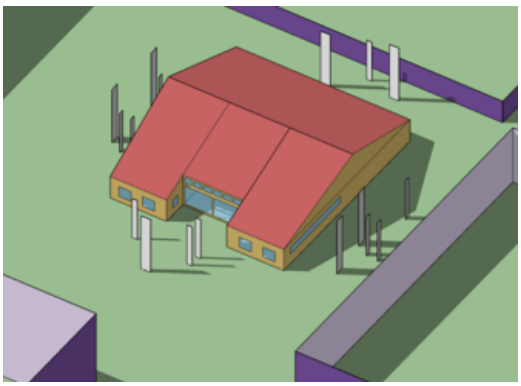

(a) Geometry model in SketchUp

(b) Exterior view

Figure 7.1: Case study building.

Figure 7.3 represents information from three typical weather.

- Typical Cold Weather: The days are warm for around two hours at noon, though the temperature is overall under the comfort zone. The climate is humid during winter months when it is cold. The higher humidity is caused by the presence of rain, sea breeze, and fog. The solar radiation is low during fall and winter; rainfall is greatest during winter. Wind direction pattern shows wind coming from the north during the nighttime and the west during the daytime.
- Typical Hot Weather: Rainfall is low. Solar radiation is the same as those during Typical Mild Weather. Often, the nighttime climate is comfortable. Wind direction is consistent throughout the year coming from the southwest. The wind blows consistently from the southwest during the daytime.
- Typical Mild Weather: During the daytime, the temperature is around 18C. Most of the day is still under comfort zone when accounting for humidity. Wind pattern is similar to that of hot weather, with strong daytime southwest wind and northbound wind during the night.

The psychrometric chart obtained using CLIMATE CONSULTANT [56] relates dry bulb temperature and humidity, which informs how the building envelope can filter the environment to provide comfort. The natural climate is comfortable 13% of the time each year. Many data points show colder weather, which is uncomfortable.

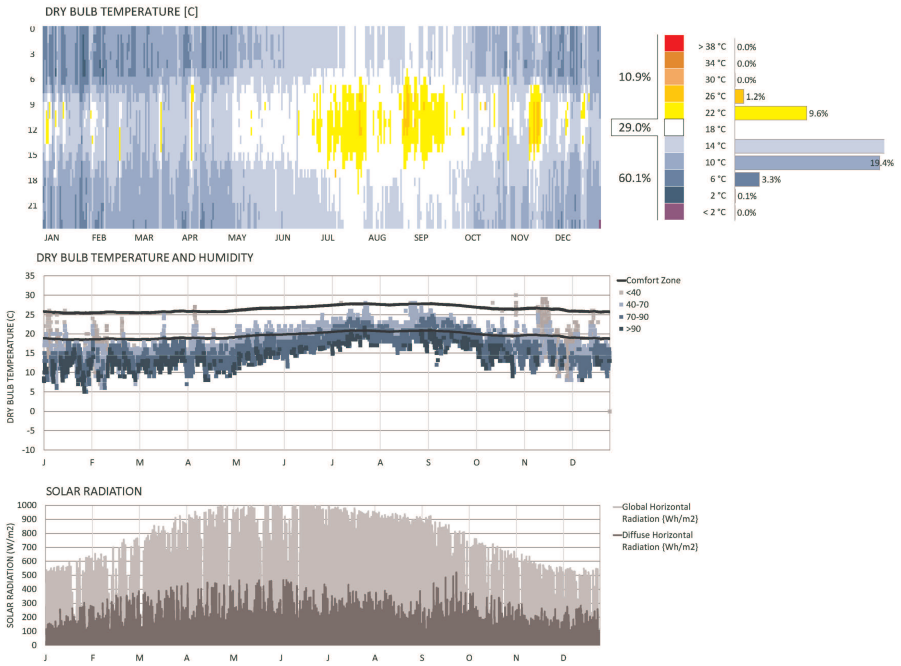

Figure 7.2: The TMY graphs of the location.

There are very few uncomfortably hot days compared to cold days. With passive design strategies in place, 86% of each year will be comfortable. Internal heat gain contributes to 65% of comfortable hours. Passive solar direct gain mass further provides warmth and comfort. To alleviate uncomfortably hot days, sun shading of windows and natural ventilation can provide an additional 3.4% of comfortable days.

7.2 Model Sensitivity Analysis

A true Building Information Model (BIM) is built to facilitate the analysis. Each piece of geometry has information embedded in it. After some simple calibration, such as materials and constructions, internal thermal loads, window glass and frames, the baseline model is refined to reflect the real scenario.

This sensitivity analysis is conducted by simulating exaggerated values of the baseline model in order to find which categories of energy use are most sensitive to change. The more sensitive categories should then be prioritized because they are

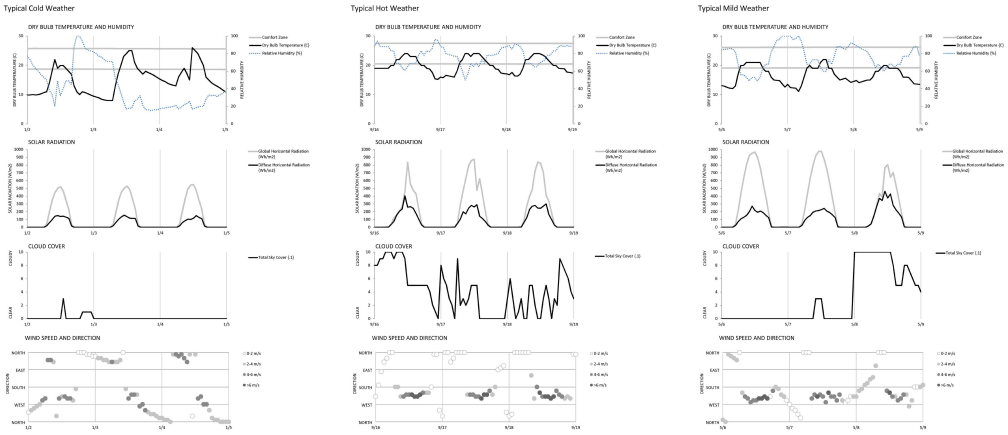

Figure 7.3: The representative typical weather information.

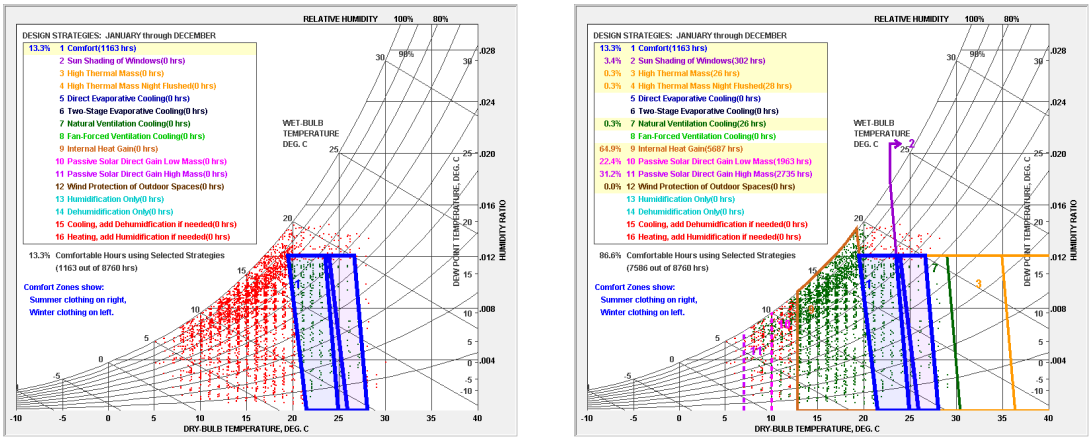

(a) Comfort chart with no strategies. (b) Comfort chart with passive strategies.

Figure 7.4: The bio-psychrometric chart.

sensitive means that minimal change will produce significant reductions in energy use.

In this analysis, whenever possible, the values of the baseline were tripled; by increasing the values by a consistent amount, the outputs will be comparable. The internal load model results for sensitivity analysis are shown in Figure 7.5. The effects of many factors are analyzed, including people, lights, equipment, process,

hot water, insulation, glass, and mass.

The only building envelope variable that seems to impact the building significantly is infiltration, which is very sensitive to change. However, infiltration does not increase energy usage more than internal loads, given that the building is primarily used as an office/working space, which is highly dependent on office equipment. Additionally, the climate is relatively mild, which makes the changes to the building envelope having a smaller impact on the overall energy usage of the building. Therefore, we can prioritize optimizing energy usage for the internal loads to minimize the buildings energy demand.

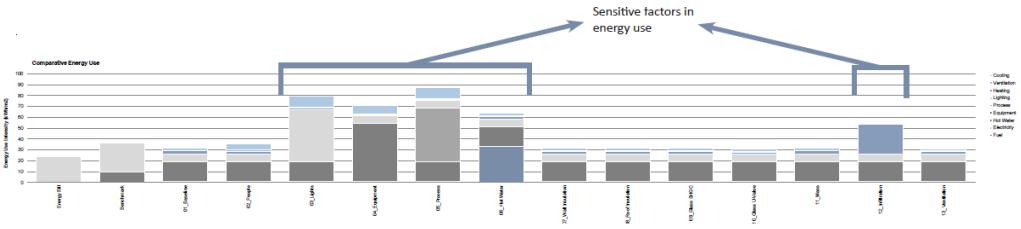

Figure 7.5: The comparative energy use for sensitivity analysis.

7.3 Mixed-mode ventilation

Heating and cooling

The simulation will be run multiple times to evaluate the HVAC systems. Figure 7.6 shows the heating and cooling energy use based on the specified use of equipment. There exists an opportunity to reduce cooling through natural ventilation during the hot weather.

No ventilation

If there is no ventilation and heating at all, the preliminary analysis 7.7 shows the unconditioned building is comfortable 65.5% of the year. There is significant overheating from April to November, which means that there is a high potential for ventilation to help cool the building during that time.

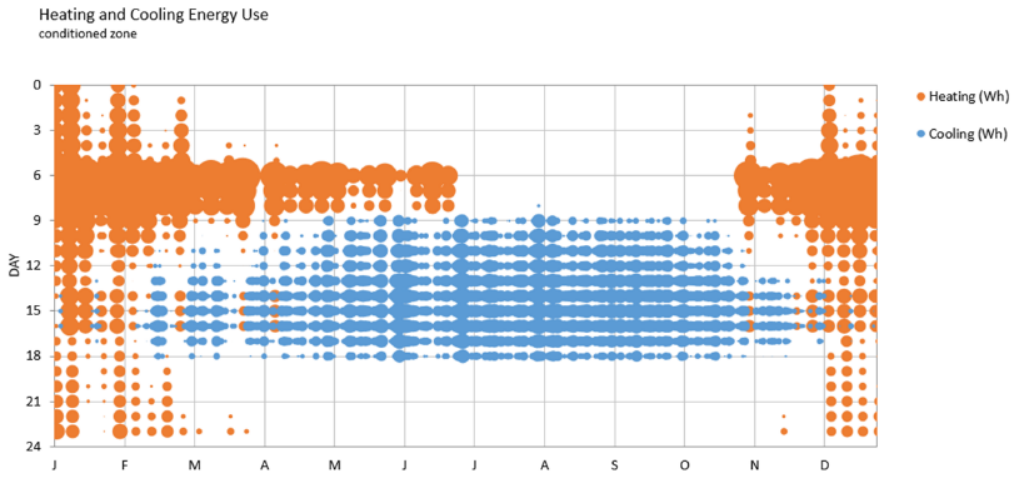

Figure 7.6: The heating and cooling energy use for conditioned zone.

Natural ventilation only

We need to access the building's potential to take advantage of natural ventilation. Figure 7.8 shows how the wind flows through the building via operable doors and windows. The heat maps of the thermal autonomy 7.9 indicate that using natural ventilation is not enough to cool down the building during hot days.

Mixed-mode schedule

It is cost-effective to combine natural ventilation with mechanical ventilation. The natural ventilation is desirable when the outside air temperature is lower than indoors, and the outside air temperature has relatively low humidity. As seen in Figure 7.7, the period of overheating occurs during 12pm-9pm from April 1 to November 1. While the period of desirable natural ventilation occurs during 9am-3pm from April 1 to November 1.

With the corresponding heating, cooling, and natural ventilation availability schedule, the mixed-mode ventilation yields the following result 7.10. The mixed mode model appears to be a better option because it produces the highest percentage of comfortable time during occupied hours.

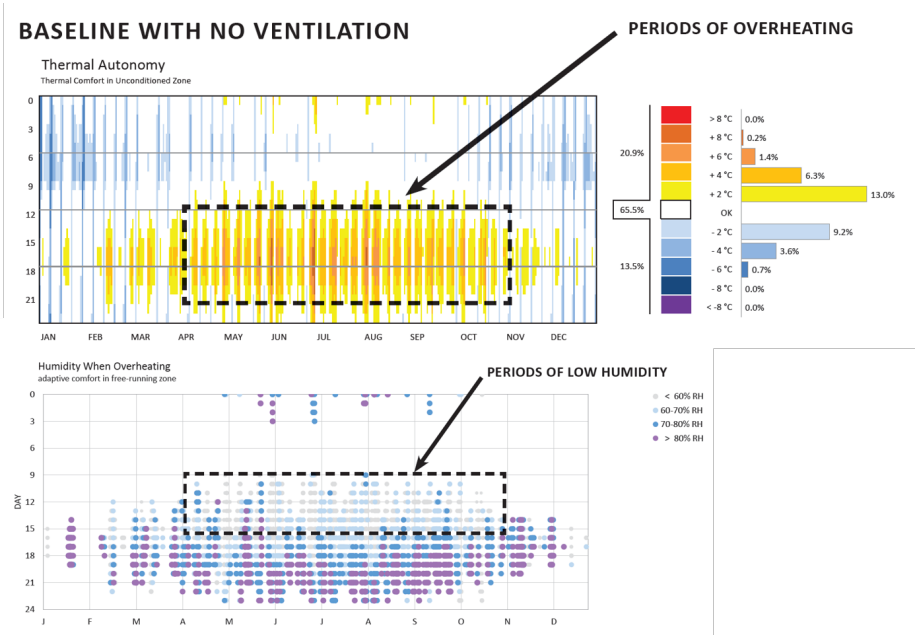

Figure 7.7: The baseline model with no ventilation.

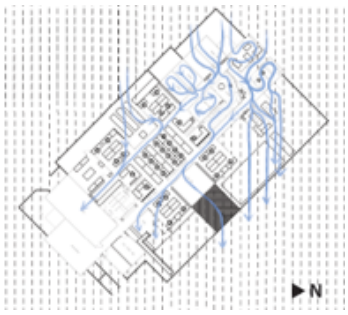

Figure 7.8: The airflow diagram through the openings.

7.4 Comfort suites

In this section, more energy-efficient upgrade measures are explored to reduce the energy use further. The lights, equipment, appliances, and hot water are replaced with more efficient models. The windows are replaced with lower U-value glass, and the current envelope is repaired to allow less infiltration. The comparative energy

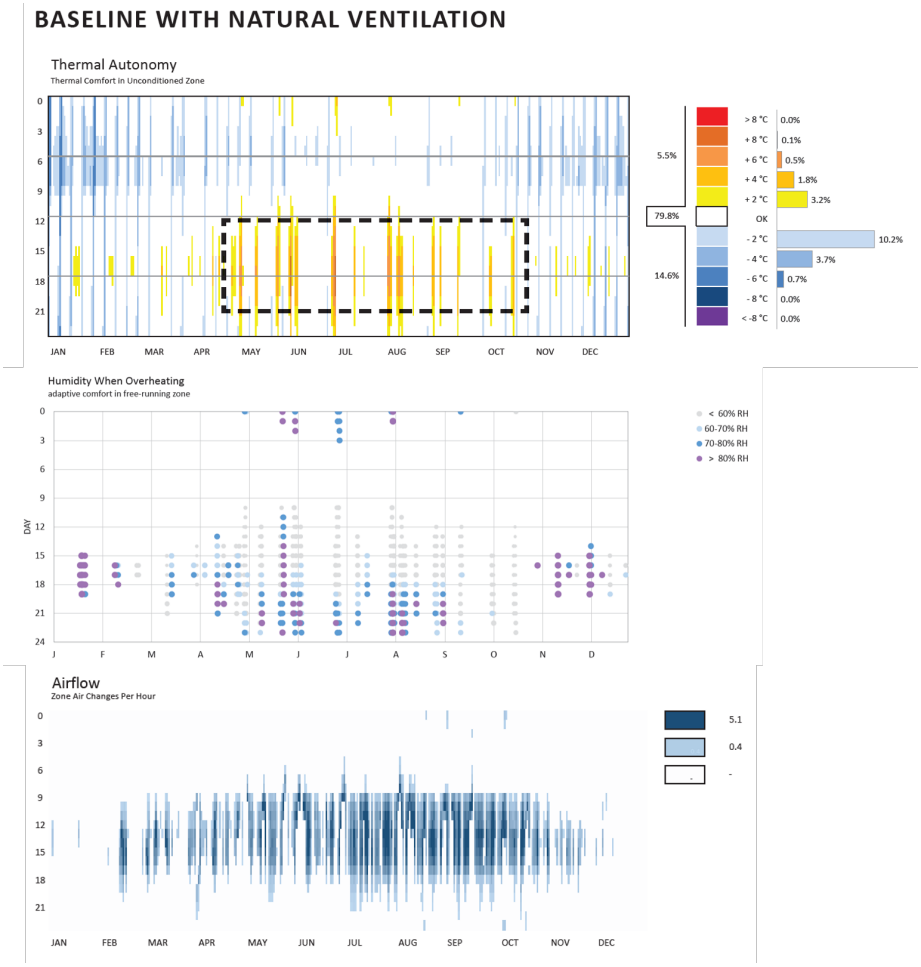

Figure 7.9: The baseline model with only natural ventilation.

use is shown in Figure 7.11 with the corresponding thermal comfort chart in Figure 7.12.

The heating increases after reducing the equipment since the more efficient appliances generate less heat, and then decreases after windows are replaced with lower U-value. However, once the glass insulation increases, the cooling also increased, which is not enough to counteract the decrease of energy in heating. Therefore, improving lighting and glass made the most impact on overall energy use.

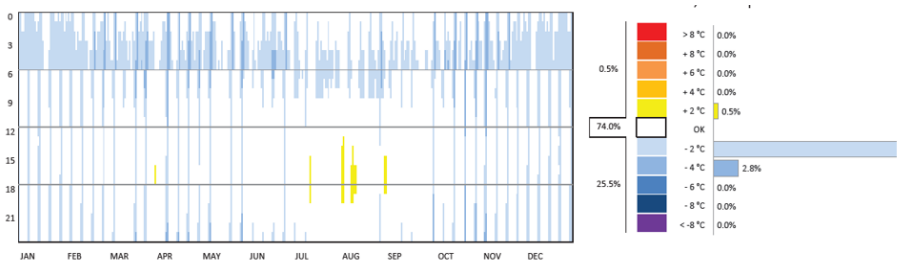

Figure 7.10: The heat maps of comfortable temperature using the mixed-mode ventilation.

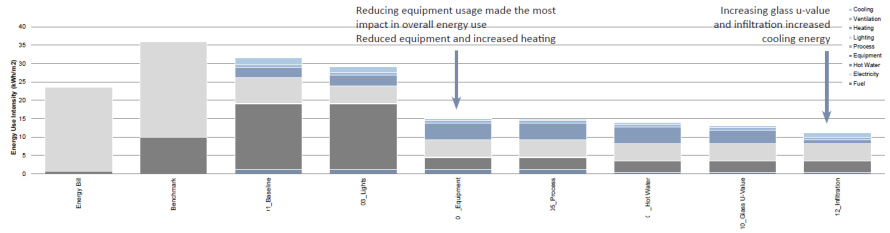

Figure 7.11: The comparative energy use for the proposed comfort suite.

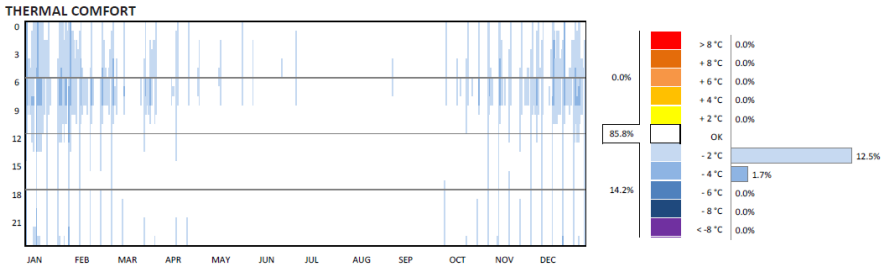

Figure 7.12: The thermal comfort chart for the proposed comfort suite.

7.5 On-site renewable energy

In this study, the diurnal and seasonal change of the ambient temperature within this particular building structure and surroundings are investigated. Figure 7.13 indicates that the front of the building is consistently well lit throughout the year,

and the back of the building is consistently shaded. And the optimal configuration for the roof solar panels is found to having a tilt of 10 degrees from the current configuration, which produce the most amount of energy.

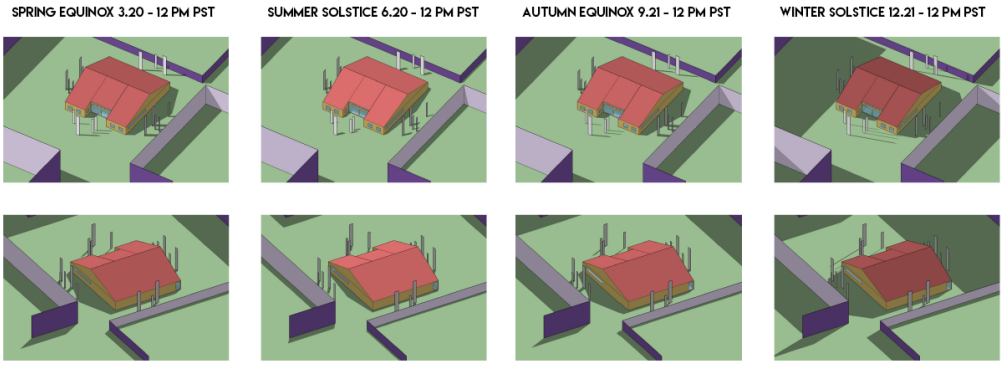

Figure 7.13: The sun exposure study among the year.

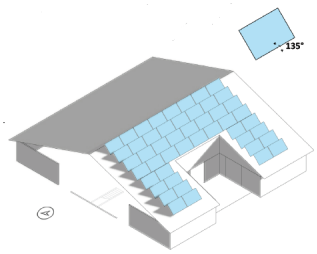

Figure 7.14: The optimal configuration of solar panels.

The energy generated by the solar panels is on an hourly basis, as seen in Figure 7.15. The energy production density is condensed between the intervals of March through October. From Figure 7.16, the building can produce enough energy to be net positive in Spring, Summer, and Fall.

7.6 Summary

In this chapter, an existing office building is analyzed for energy use, and appropriate measures are proposed to improve performance. It entails an energy audit

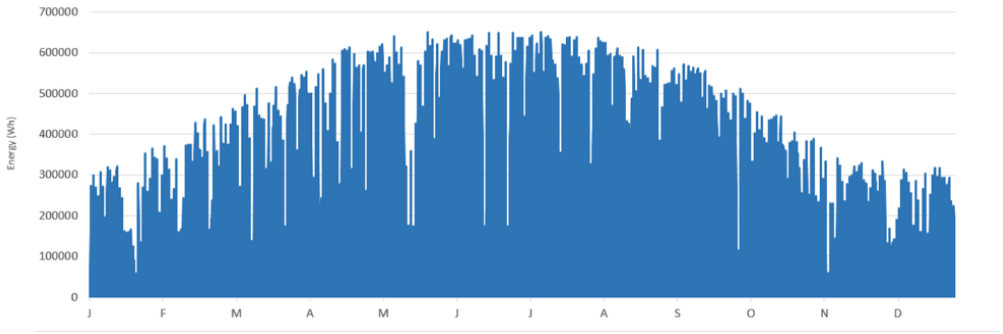

Figure 7.15: On-site energy generation.

and reports the value of energy-efficient measures. The project focuses on parametric methods of analyzing benefits and value in terms of cost, comfort, and energy. More specifically, the mixed-mode ventilation is explored to take the most benefits of natural ventilation. On-site renewable energy is investigated to achieve net zero energy building.

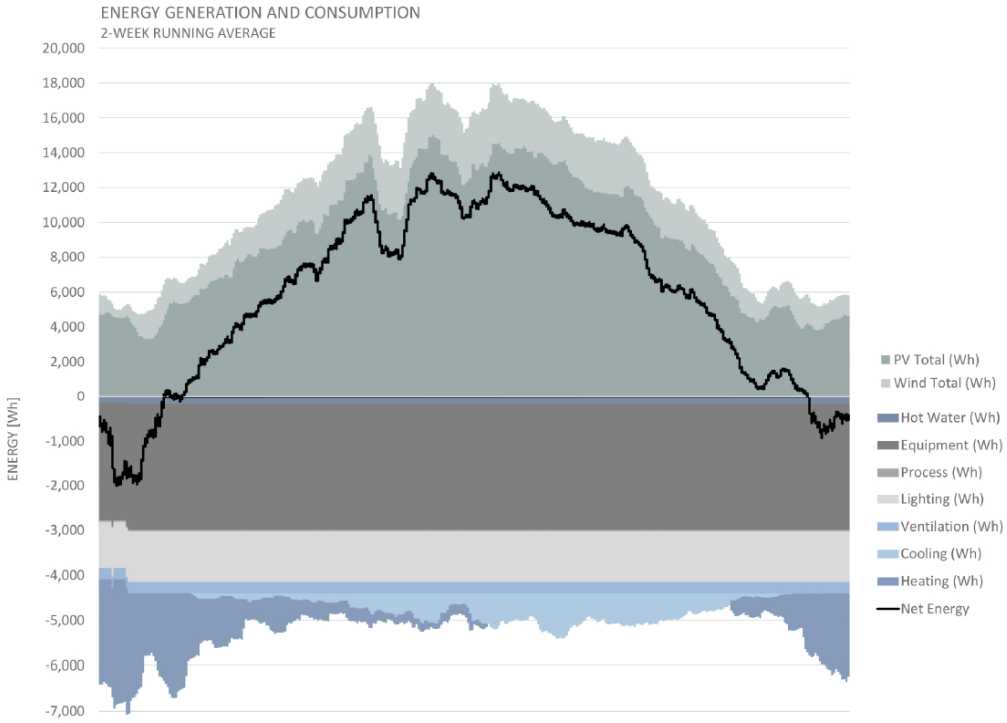

Figure 7.16: The energy generation and consumption through the year.

Bibliography

[1] Energy Information Administration. *U.S. Department of Energy*. `http://www.eia.gov/totalenergy/`. [Online].

[2] EGB Workgroup. *Buildings and their impact on the environment: a statistical summary*. Tech. rep. Technical Report, US Environmental Protection Agency, 2009.

[3] Architecture 2030. `http://architecture2030.org/`. [Online].

[4] U.S. General Services Administration. *Benefits of Green Buildings on Costs, the Environment and Jobs*.

[5] Norbert Lechner. *Heating, cooling, lighting: Sustainable design methods for architects*. John wiley & sons, 2014.

[6] Paul Torcellini et al. "Zero energy buildings: a critical look at the definition". In: *National Renewable Energy Laboratory and Department of Energy, US* (2006).

[7] Anna Joanna Marszal et al. "Zero Energy Building, A review of definitions and calculation methodologies". In: *Energy and buildings* 43.4 (2011), pp. 971–979.

[8] Patxi Hernandez and Paul Kenny. "From net energy to zero energy buildings: Defining life cycle zero energy buildings (LC-ZEB)". In: *Energy and Buildings* 42.6 (2010), pp. 815–821.

[9] S Taylor, TJ Stein, and G Paliaga. "Design guidelines: Advanced variable air volume (VAV) systems". In: *Energy Design Resources, California Energy Commission* (2009).

[10] S Taylor. "Resetting setpoints using trim & respond logic". In: *ASHRAE Journal* (2015), pp. 52–57.

[11] Tyler Hoyt, Edward Arens, and Hui Zhang. "Extending air temperature setpoints: Simulated energy savings and design considerations for new and retrofit buildings". In: *Building and Environment* 88 (2015), pp. 89–96.

[12] Edward Arens et al. "Thermal and Air Quality Acceptability in Buildings that Reduce Energy by Reducing Minimum Airflow from Overhead Diffusers". In: (2013).

[13] Gwelen Paliaga. "Dual maximum VAV box control logic". In: *ASHRAE Journal* 54.12 (2012), p. 16.

[14] JE Seem and JM House. "Development and evaluation of optimization-based air economizer strategies". In: *Applied Energy* 87.3 (2010), pp. 910–924.

[15] ASHRAE. "Standard 55-2016 Thermal Environmental Conditions for Human Occupancy". In: *ASHRAE Standard* (2016).

[16] ASHRAE. "Standard 62.1-2016 ventilation for acceptable indoor air quality". In: *ASHRAE Standard* (2016).

[17] ASHRAE. "Standard 90.1-2016 Energy standard for buildings except low-rise residential buildings". In: *ASHRAE Standard* (2016).

[18] California Energy Commission. *California Title 24*. `http://www.energy.ca.gov/title24/`. 2016.

[19] Anil Aswani et al. "Reducing transient and steady state electricity consumption in HVAC using learning-based model-predictive control". In: *Proceedings of the IEEE* 100.1 (2012), pp. 240–253.

[20] Yudong Ma, Garrett Anderson, and Francesco Borrelli. "A distributed predictive control approach to building temperature regulation". In: *American Control Conference (ACC), 2011*. IEEE. 2011, pp. 2089–2094.

[21] Mehdi Maasoumy and Alberto Sangiovanni-Vincentelli. "Total and peak energy consumption minimization of building hvac systems using model predictive control". In: *IEEE Design & Test of Computers* 29.4 (2012), pp. 26–35.

[22] Frauke Oldewurtel et al. "Use of model predictive control and weather forecasts for energy efficient building climate control". In: *Energy and Buildings* 45 (2012), pp. 15–27.

[23] Olivier Van Cutsem et al. "Comparison of MPC Formulations for Building Control under Commercial Time-of-Use Tariffs". In: *IEEE PowerTech Milan 2019*. 2019 2019.

[24] David Blum et al. "Practical factors of envelope model setup and their effects on the performance of model predictive control for building heating, ventilating, and air conditioning systems". In: *Applied Energy* 236 (Feb. 2019), pp. 410–425. ISSN: 03062619.

[25] Yudong Ma. *Model predictive control for energy efficient buildings*. University of California, Berkeley, 2013.

[26] Petru-Daniel Moroşan et al. "Building temperature regulation using a distributed model predictive control". In: *Energy and Buildings* 42.9 (2010), pp. 1445–1452.

[27] Alex Beltran and Alberto E. Cerpa. "Optimal HVAC Building Control with Occupancy Prediction". In: *Proceedings of the 1st ACM Conference on Embedded Systems for Energy-Efficient Buildings*. BuildSys fffdfffdfffd14. Memphis, Tennessee: Association for Computing Machinery, 2014, 168fffdfffdfffd171. ISBN: 9781450331449.

[28] June Young Park et al. "A critical review of field implementations of occupant-centric building controls". In: *Building and Environment* 165 (2019), p. 106351. ISSN: 0360-1323.

[29] Iakovos T. Michailidis et al. "Proactive control for solar energy exploitation: A german high-inertia building case study". In: *Applied Energy* 155 (2015), pp. 409–420. ISSN: 0306-2619. DOI: https://doi.org/10.1016/j.apenergy.2015.06.033. URL: http://www.sciencedirect.com/science/article/pii/S0306261915007916.

[30] Comfy. https://comfyapp.com/.

[31] U.S. Department of Energy. "Operations and Maintenance Best Practice: A Guide to Achieving Operational Efficiency". In: (2010).

[32] Ran Liu et al. "Stability and accuracy of variable air volume box control at low flows. Part 1: Laboratory test setup and variable air volume sensor test". In: *HVAC&R Research* 20.1 (2014), pp. 3–18.

[33] Mark Hydeman et al. "Advanced variable air volume system design guide". In: *California Energy Commission* (2003).

[34] http://www.trnsys.com/.

[35] https://energyplus.net/.

[36] http://simulationresearch.lbl.gov/modelica/.

[37] A Mechaqrane and M Zouak. "A comparison of linear and neural network ARX models applied to a prediction of the indoor temperature of a building". In: *Neural Computing & Applications* 13.1 (2004), pp. 32–37.

[38] Center For the Built Environment. *Occupant Survey Toolkit*. https://cbe.berkeley.edu/resources/occupant-survey/.

[39] CBE Thermal Comfort Tool. `http://comfort.cbe.berkeley.edu/`. Center for the Built Environment, University of California Berkeley. 2017.

[40] Bud Offermann. "The IAQ Top 10". In: (2008).

[41] Anthony Kelman, Yudong Ma, and Francesco Borrelli. "Analysis of local optima in predictive control for energy efficient buildings". In: *Journal of Building Performance Simulation* 6.3 (2013), 236–255.

[42] USGBC. *LEED v4*. `https://new.usgbc.org/leed`.

[43] Kaiyu Sun et al. "Stochastic modeling of overtime occupancy and its application in building energy simulation and calibration". In: *Building and Environment* 79 (2014), pp. 1–12.

[44] `http://www.brcm.ethz.ch/doku.php`.

[45] Datong P. Zhou, Qie Hu, and Claire J. Tomlin. "Model Comparison of a Data-Driven and a Physical Model for Simulating HVAC Systems". In: *ArXiv* abs/1603.05951 (2016).

[46] Stephen Dawson-Haggerty et al. "sMAP: a simple measurement and actuation profile for physical information". In: *Proceedings of the 8th ACM Conference on Embedded Networked Sensor Systems*. ACM. 2010, pp. 197–210.

[47] Anil Aswani et al. "Identifying models of HVAC systems using semiparametric regression". In: *American Control Conference (ACC), 2012*. IEEE. 2012, pp. 3675–3680.

[48] Q. Hu et al. "Building model identification during regular operation - empirical results and challenges". In: *2016 American Control Conference (ACC)*. 2016, pp. 605–610. DOI: `10.1109/ACC.2016.7524980`.

[49] Giuseppe C Calafiore, Laurent M El Ghaoui, and Carlo Novara. "Sparse identification of posynomial models". In: *Automatica* 59 (2015), pp. 27–34.

[50] Slowness Principle. "Slow Feature Analysis". In: (2014).

[51] J. Stein M. Hydeman. "A fresh look at fans: preliminary findings from California research project provide insight into fan design and energy savings". In: *Heat. Pip. Air Cond. Eng. 5* 5 (2003).

[52] Paul Raftery et al. "Evaluation of a cost-responsive supply air temperature reset strategy in an office building". In: *Energy and Buildings* 158 (2018), pp. 356–370. ISSN: 0378-7788.

[53] OpenBMS. `http://www.openbms.org/dashboard/`.

[54] Jessica Granderson et al. "Accuracy of automated measurement and verification (M&V) techniques for energy savings in commercial buildings". In: *Applied Energy* 173 (2016), pp. 296–308.

[55] Jungsuk Kwac, June Flora, and Ram Rajagopal. "Household energy consumption segmentation using hourly data". In: *Smart Grid, IEEE Transactions on* 5.1 (2014), pp. 420–430.

[56] *Climate Consultant*. `http://www.energy-design-tools.aud.ucla.edu/`.